Distribution Agreement

In presenting this thesis or dissertation as a partial fulfillment of the requirements for an advanced degree from Emory University, I hereby grant to Emory University and its agents the non-exclusive license to archive, make accessible, and display my thesis or dissertation in whole or in part in all forms of media, now or hereafter known, including display on the world wide web. I understand that I may select some access restrictions as part of the online submission of this thesis or dissertation. I retain all ownership rights to the copyright of the thesis or dissertation. I also retain the right to use in future works (such as articles or books) all or part of this thesis or dissertation.

Signature:

_____ _____

David Painton Bray Date

Functional, genomic, and radiographic associations with outcomes in *IDH*-mutant glioma: experience from a high-volume tumor center

By

David Painton Bray, M.D.

Master of Science

Clinical Research

_____
Jeffrey J. Olson, M.D.
Advisor

_____
Tomas Garzon-Muvdi, M.D., MSc
Committee Member

_____
Jordan Kempker, M.D., MSc
Thesis Chairperson

Accepted:

_____
Kimberly Jacob Arriola, Ph.D, MPH
Dean of the James T. Laney School of Graduate Studies

_____
Date

Functional, genomic, and radiographic associations with outcomes in *IDH*-mutant glioma: experience from a high-volume tumor center

By

David Painton Bray

B.A., University of Notre Dame, 2011

M.D., Columbia University, College of Physicians and Surgeons, 2016

Advisor: Jeffrey J. Olson, M.D.

An abstract of a thesis submitted to the Faculty of the James T. Laney School of Graduate Studies of Emory University in partial fulfillment of the requirements for the degree of Master of Science in Clinical Research

2023

Abstract

Functional, genomic, and radiographic associations with outcomes in *IDH*-mutant glioma:

experience from a high-volume tumor center

By: David P. Bray, M.D.

Introduction:
Gliomas are tumors that arise from brain tissue. While the most common tumors are high-grade and diagnosis portends a poor prognosis, a recently-defined subset of glioma characterized by a mutation of isocitrate dehydrogenase gene (*IDH*-mutant) are low/intermediate grade. *IDH*-mutant gliomas represent a heterogenous group of tumors with differing outcomes. We have one of the largest single-institution experiences with patients with *IDH*-mutant glioma. The goal of this project was describe frailty, tumor genetic, and radiographic parameters that relate to outcomes within *IDH*-mutant glioma.

Methods:
We had three aims in defining outcomes within our *IDH*-mutant glioma cohort. We first collected frailty-specific measures and calculated Charlson Comorbidity Index (CCI) and 5-factor modified frailty index (mFI-5). We tested this as an exposure for outcomes of 30-day readmission and overall survival. For the second aim, we tested the exposure of copy number (CN) variation, a proxy for mutational burden within the tumor, for outcomes of overall survival and progression free survival. Finally, we created and compared deep-learning, neural-network algorithms with non-imaging and MR imaging-only parameters to predict the outcome for genetic lineage of *IDH*-mutant glioma (astrocytoma vs. oligodendroglioma).

Results:
Higher frailty was not associated with 30-day readmission, nor overall survival in our cohort of *IDH*-mutant glioma patients, except when their first operation was performed at our institution. Higher CN variation was associated with lower progression free survival. We were able to predict astrocytoma vs. oligodendroglioma lineage using our deep-learning, neural-network algorithm. The MR imaging-only parameters better predicted tumor type than non-imaging variables.

Conclusion:
We further described the roles of frailty, tumor genetics, and imaging-predicting exposures within our single-institution experience of *IDH*-mutant glioma. Most of our statistical analyses were underpowered to define meaningful associations, however, these findings may inform future, larger cohort analyses.

Functional, genomic, and radiographic associations with outcomes in *IDH*-mutant glioma: experience from a high-volume tumor center

By

David Painton Bray

B.A., University of Notre Dame, 2011

M.D., Columbia University, College of Physicians and Surgeons, 2016

Advisor: Jeffrey J. Olson, M.D.

A thesis submitted to the Faculty of the James T. Laney School of Graduate Studies of Emory University in partial fulfillment of the requirements for the degree of

Master of Science in Clinical Research

2023

Acknowledgements

I would like to thank and acknowledge Dr. Jeffrey J. Olson and Dr. Kimberly B. Hoang for their mentorship on this project and support through the Master of Science program.

I would like to thank Dr. Stewart Neill (Neuropathology), Dr. Jeffrey Switchenko (Biostatistics and Bioinformatics), and Manali Rupji (Biostatistics and Bioinformatics) for their assistance in the design and analysis of this project.

Thank you to Dr. Jordan Kempker (thesis advisor) and the rest of the MSCR program for their guidance over the last 2 years.

Finally, thank you to my wife, Morgan, and my two daughters (Madeleine and Sophia) for their support and patience through this degree process and my neurosurgical training.

Table of Contents

Introduction:

Intracerebral gliomas represent one of the most common, yet feared entities within neuro-oncology.[1] Gliomas represent a large spectrum of clinical outcomes for patients depending on patient related factors (i.e. age/medical comorbidities), tumor location/size upon diagnosis, and pathological/genetic characteristics of the tumor. A major effort on the part of neuro-oncological researchers for the last 20 years has been to define the genetic underpinnings of specific gliomas within this diverse array of neuro-oncological disease.[1–4] Certainly, akin to other efforts within the larger oncology research field to genetically-define tumors, researchers have discovered that genetic categorization of gliomas has yielded superior prognostication schema for survival and response to current therapies.[5] Additionally, elucidating genetic signatures of glioma has allowed for a myriad trials of targeted therapeutics in an attempt improve the prognosis for this disease.[6]

High grade gliomas (HGG) are World Health Organization (WHO) grade 3 and 4 gliomas that are characterized by aggressive growth, elevated recurrence rates, and poor prognosis.[7,8] Within HGGs, researchers have identified mutations in isocitrate dehydrogenase (*IDH*) that divide HGGs into more aggressive and less aggressive entities.[2,9] Patients with *IDH*-mutant glioma have a better prognosis than their *IDH*-wild-type counterparts in terms of time to recurrence and overall survival.[10] However, there are multiple, unique sub-categorizations of patient populations within *IDH*-mutant gliomas that are yet to be well-defined. For example, sub-classification based on cyclin-dependent kinase inhibitor 2 (*CDKN2A/B*) may allow clinicians to better stratify patients within the *IDH*-mutant glioma cohort.[11] Over the last 5-8 years, neuropathologists have switched from histopathological classification to genetically-based definitions of cohorts within the heterogenous group of patients within *IDH*-mutant glioma.[11] However, there remains a

paucity of surgical, patient-level data to investigate how these molecularly-defined cohorts within *IDH*-mutant glioma relate to radiographic findings, pre-existing medical comorbidities, surgical outcomes, and response to targeted therapies.

The CNS Tumor Outcomes Registry at Emory (CTORE) and CLInical Neurosurgery Outcomes Investigations Database (CLINOID) are two, multi-institutional and inter-disciplinary clinical databases that have been created to study outcomes of patients with neurosurgical oncological pathology. Our neuropathology team has completed advanced genetic analysis of all gliomas operated upon at our institution since 2007; well before WHO guidelines recommended defining glioma by genetic signatures in 2016. Therefore, our group has one of the largest, single institution experiences in the surgical management of *IDH*-mutant glioma. Our experience provides our research group a unique opportunity to further define patients within the *IDH*-mutant glioma subgroup.

We created three aims to best define groups within *IDH*-mutant glioma. First, we defined surgical outcomes with frailty indices as an exposure. Next, we investigated whether genetic microarray data could be correlated with patient overall survival and tumor recurrence. Last, employing a convolutional, adaptive neural network, we related specific magnetic resonance imaging (MRI) based parameters to predict *IDH*-mutant tumor type.

Background:

<u>HGGs are a common CNS neoplasm and portend a poor prognosis:</u>

Gliomas are some of the most common CNS neoplasms and they arise from the brain parenchyma. They are subdivided into four different grades by the WHO.[7] Classically, gliomas were defined by histopathological parameters, but they are increasingly defined by their unique genetic code.[12] HGGs are defined as WHO grade III and IV gliomas. They represent approximately 60-75% of all new diagnoses of glioma.[7] Patients commonly present with new neurological deficits, confusion, or with seizure.

The gold standard for treatment of HGG is maximal safe neurosurgical resection of the bulk of the tumor, followed by adjuvant concomitant temozolomide chemotherapy and radiotherapy.[13,14] Due to the infiltrating nature of gliomas, gross total resection of the entirety of tumor after presentation is impossible.[15] Infiltrating tumor cells reach far outside the tumor bulk, are incompletely resected in surgery (even after "gross total resection" of identified tumor on preoperative imaging). Recurrences of tumor are thought to arise at the populations of infiltrating cells.[16] HGGs are a "local" tumor and very rarely metastasize via the lymphatics or bloodstream.[5] Despite aggressive treatment, the median survival of HGG is dismal with WHO grade IV glioma survival having a median 13 months, and WHO grade III survival at a median of 26 months.[6]

HGGs represent a diverse spectrum of genetic types that correspond to differing survival expectancies for patients. They are thought to be derived from de-differentiated neural stem cells that manifest a conglomerate of accumulated mutations that vary within and between tumors.[5] The diversity of tumor cell types within a single patient's unique HGG likely contributes to the

ineffectiveness of their adjuvant treatment.[7] There have been many attempts at treating HGGs with chemotherapies, immunotherapies, and different radiation schema. HGGs have demonstrated that they are able to evade treatments by utilization of alternative proliferative pathways and creating immunosuppressive microenvironments that allow for proliferation of tumor cells without the surveillance of the endogenous immune system.[8,9] Researchers hope that with further sub-categorization of HGG types neuro-oncologists and neurosurgeons may be able to better determine patient prognosis, and develop novel treatments for different HGG types.[3]

IDH-mutant gliomas represent a heterogenous entity within HGGs:

The diversity of HGG type contributes to their resistance to therapies, their high recurrence rates, and reduced overall survival.[4] As previously mentioned, recent efforts of neuropathologists working in HGG research has been dedicated to the subclassification of HGG type by their genetic signature.[10] Researchers have identified *IDH*-mutation as one such subclassification that has major implications for prognostication and possibly for different potential avenues for treatment.[11–13] HGGs with *IDH*-mutations more commonly occur in younger patients, as well as in HGG patients with "secondary glioblastoma;" a HGG that has developed from a previously present lower grade glioma.[1] Secondary HGGs often harbor p53 mutations, while "primary" HGGs tend to present in older individuals and have more mutations in *EGFR* and *PTEN*.[1]

The presence of an *IDH*-mutation in both WHO grade III and IV HGGs portends a better prognosis, and the use of *IDH*-typing has been a powerful tool for predicting outcomes for patients with HGGs. Gliomas that were histopathologically-defined as lower grade gliomas

without *IDH*-mutation ("*IDH*-wildtype") have been shown to have similar recurrence rates and overall survival to WHO grade IV glioblastoma.[14] It is now clear that there are subtypes of *IDH*-mutant gliomas based on additional genetic abnormalities present across that tumor population.[15–17] Reuss et al. investigated *IDH*-mutant gliomas at their institution and discovered two variants of *IDH*-mutant glioma: *IDH*-mutant glioma with 1p/19q chromosome co-deletion (termed "oligodendroglioma") and *IDH*-mutant glioma with *ATRX*-loss (termed "diffuse astrocytoma").[15] Oligodendrogliomas arise from oligodendrocytes and diffuse astrocytomas are from astrocytic origin; these distinct genetic signatures correlate to their CNS cell of origin. Subtyping by these genetic signatures offers superior prognosis grouping than previously-employed histopathological definitions of HGGs.[18] Oligodendrogliomas have the best overall outcome of all gliomas, and diffuse astrocytomas have a better prognosis compared to *IDH*-wildtype HGGs.

There may be additional subclassifications within *IDH*-mutant oligodendroglioma and astrocytoma that have implications for prognosis, treatment, and surgical decision making. For example, *MGMT* methylation predicts response to the alkylating-chemotherapeutic used to treat HGGs, temozolimide.[19] Homozygous loss of *CDKN2A/B* identifies a more aggressive variant of IDH-mutant glioma.[20–22] Quantifying the number of point mutations or CN variations within a glioma may be useful in estimating the overall genomic instability of a tumor.[16,23–25] Recently, there has been evidence that these biomarkers will have specific implication for surgical decision-making. For example, Nakae et al. identified that *IDH*-mutant oligodendrogliomas tended to recur locally, near the original resected tumor location, while *IDH*-mutant gliomas with p53 mutations recurred in remote intracranial locations.[26] These data are helpful for

neurosurgeons as they can assist identifying which patients may be candidates for additional cytoreductive surgery, and determine candidacy for additional therapies. This will address the paucity of patient-level surgery data for the *IDH*-mutant glioma population.[27]

Aim 1: Frailty indices and *IDH*-mutant glioma

By the year 2050, the United States (US) is projected to have 83.7 million individuals aged over 65; almost double that which was projected for the year 2012.[28] As the US and world population ages, neurosurgeons may encounter increasing numbers of gliomas. Additionally, due to aging population, there may be more glioma patients that need aggressive operations at older ages and with more medical comorbidities. *IDH*-mutant gliomas represent a diverse range of tumors that have median survivals that range from 18 months to greater than 10 years.[2,3,14]

While the concept of "frailty" and its impact upon medical/surgical care has been present for over 30 years, it has only recently been applied to prognostication of outcome after neurosurgical treatment.[29,30] "Frailty" has been defined as a patient's ability to respond to a given stressor.[31] In the neuro-oncological literature, frailty has been used to predict surgical decision-making in geriatric patients with WHO grade IV glioma,[32] 30-day readmission in patients undergoing cranial neuro-oncological procedures,[33] and increases in hospital charges during neuro-oncological hospitalizations.[34] In sum, neurosurgical studies about frailty in neuro-oncology have focused on frailty as an exposure variable in glioblastoma and other more common cranial tumor-types, where it has been associated with worsened outcomes. However, there are no studies that have studied the impact of frailty in patients with *IDH*-mutant glioma. This is due to

the recent reclassification of WHO glioma grading, and lack of experience with this specific pathology. It is unclear whether increased frailty is associated with worsened outcomes in patients with *IDH*-mutant glioma (like in other intracranial tumor types), or if other tumor-related factors, such as tumor genetics or size/location, matter more.

Aim 2: Copy number (CN) variations and *IDH*-mutant gliomas

There is increasing evidence that CN alteration burden within *IDH*-mutant gliomas may have implications for patient prognosis within this cohort. Richardson et al. described a population of *IDH*-mutant gliomas that had an unexpected poor prognosis, more akin to an *IDH*-wildtype glioma.[24] These more aggressive *IDH*-mutant gliomas were found to harbor an increased CN alterations, though there was no group of shared epigenetic themes between the tumors. The authors concluded that increased CN mutations may be a proxy for genomic instability of the tumor. They continued this research in *IDH*-mutant astrocytomas and found a similar phenomenon.[25] Shirahata et al. described a novel grading system for *IDH*-mutant gliomas that included CN variant mutational burden, and found CN alterations to relate to prognosis more than mitotic indices on histopathological analysis.[35] Others have corroborated this data.[36,37] While these groups have related overall survival of patients to these pathological parameters, there is a lack of surgery and radiographic patient-level data and this is needed to contribute to the growing interest and literature on CN alterations to make this information more clinically relevant.

Aim 3: Radiographic parameters

Gliomas are extensively quantified by their pathological genomic signature. The gold standard for imaging gliomas remains magnetic resonance imaging (MRI) of the brain. From diagnosis, to surgery, to radiation, and for monitoring for recurrence, gliomas are imaged with MRI. Therefore, for each patient with a glioma, there is a large amount of radiographic data as the glioma is treated and inevitably progresses to recurrence.

"Radiomics" involves the quantification of MRI features such that they can be studied in conjunction with patient level data.[38] "Radiogenomics" is a growing discipline within radiomics that links imaging data with genomic data.[39] Radiogenomics has been applied to multiple oncological sub-disciplines, including cancers of the breast, prostate, and lung. There is a large effort to correlate clinical outcomes with radiological and genomic features in glioma as well.[40] Gutman et al. provided one of the first forays into radiogenomic analysis for glioma when they found that two variants of glioblastoma (mesenchymal and proneural) had distinct contrast enhancement patterns. Researchers have demonstrated in a xenograft mouse model that transformation and changes in the genetics of a glioma had a reproducible radiographic correlate.[41] Castet et al. correlated contrast enhancement type to increased risk of progression of low grade gliomas to HGGs.[42] There has been little research investigating radiogenomics of *IDH*-mutant gliomas.

There are MR imaging findings that correlate with *IDH*-mutant glioma type (astrocytoma vs. oligodendroglioma).[43] Oligodendroglioma have calcifications on computed tomography scans, hyperintensity upon T2-weighted (T2W) and fluid-attenuated inversion recovery (FLAIR), and

little to no enhancement upon administration of gadolinium contrast. Astrocytoma have T2W/FLAIR mismatch (more intensity upon T2W than FLAIR), no calcifications, and little to no contrast enhancement with gadolinium contrast. This allows for investigation in predicting tumor type by preoperative imaging. Identification of *IDH*-mutant tumor type in the preoperative setting could lead to differing treatment algorithms which could affect patient outcome.[44]

Methods:

Study Population

This retrospective cohort study adheres to the Strengthening the Reporting of Observational Studies in Epidemiology (STROBE) reporting guidelines.

We identified patients from the Central Nervous System (CNS) Tumor Outcome Registry at Emory (CTORE), a prospectively-maintained database of patient outcomes for CNS tumors treated Emory University Hospital and Emory University Hospital, Midtown. Both hospitals contributing patients to our database are large, tertiary/quaternary care, referral, academic institutions. In this study, we included patients 18 years or older with pathological diagnosis of *IDH*-mutant glioma who underwent a neurosurgical procedure at the above institutions between 01 January 2007 to 01 January 2021. The diagnosis of *IDH*-mutant glioma was made using multimodal neuropathological technique according to latest available WHO guidelines at the time of diagnosis.[3,14,37]

Our patient flow diagram is available in **Figure 1**. Our study size was obtained by collecting all available patients for our retrospective analysis.

Ethical Considerations:

Our Institutional Review Board reviewed this study (IRB00117860 and STUDY00000332). Our review board approved the waiver of informed patient consent for this study.

Typical glioma patient care flow diagram

The initial diagnosis and care of patients with glioma is stereotyped. We pictographically demonstrate the usual clinical flow of this process in **Figure 2**.

Patients with a brain mass are discovered after they develop clinical symptoms, such as a new neurological deficit or seizure. With the ubiquity of advanced imaging systems, they can also be found incidentally during workup for another clinical complaint. After a new brain mass is found on MRI, in almost every case, a neurosurgeon is consulted for tissue biopsy obtained through attempted resection or stereotactic needle biopsy. After recovery from surgery, neuropathologists complete genomic analysis of the glioma and neurooncologists/radiation oncologists initiate adjuvant therapies (watchful waiting, chemotherapy, and/or radiotherapy). The patient undergoes a regimented MRI follow-up protocol.

Aim 1 Methods: Frailty indices and *IDH*-mutant glioma

Variables:

Main exposure:

Frailty was defined using the 5-factor modified frailty index (mFI-5)[45], and the Charlson Comorbidity Index (CCI).[46] Both of these metrics have been validated in multiple settings in the surgical and neurosurgical literature, and across surgical disciplines. Specifically, a mFI-5 $\geq$ 1 or a CCI $\geq$ 3 have been associated with poorer outcomes.[45,47–50] These scores were calculated using the preoperative comorbidity list noted in preoperative history and physical or clinic note. If the preoperative history documentation denoted any comorbidities present in the CCI or mFI-5, it was recorded in our database as a binary (i.e. yes/no) or leveled (high, medium, low) categorical variable specific to the CCI/mFI-5 metric. The mFI-5 is scored 0-5. If the patient has the comorbidity included in the index, they receive a "1" for the condition, and receive a "0" otherwise. Factors included in the mFI-5 include: functional status (1= requiring assistance with activities of daily living, 0= not requiring assistance) and history of: diabetes, chronic obstructive pulmonary disease, heart failure, or hypertension. The CCI is calculated from a sum score of 19-possible weighted conditions and is age-adjusted.[46,51] Categories include: history of HIV/AIDS, metastatic solid tumor, liver disease, lymphoma, leukemia, any tumor, diabetes with end organ damage, renal disease, hemiplegia, diabetes, ulcer disease, connective tissue disease, chronic pulmonary disease, dementia, cerebrovascular disease, peripheral vascular disease, heart failure, myocardial infarction, and age (increasing for each decade $\geq$50 years). We categorized the

patients into “higher” vs “lower” risk by the respective frailty indices, which correlates to mFI-5 ≥ 1 or a CCI ≥ 3.

Outcomes:

Our primary outcome was 30-day rehospitalization at Emory University Hospital or Emory University Hospital, Midtown. Our secondary outcome was defined as mortality date after surgery, or overall survival. The time to survival was calculated as time interval from date of surgery to outcome or censoring. Patients were censored if they were lost to follow-up. Their survival time was calculated as the interval between date of surgery and last communication. The last possible follow-up date was 9/1/2021. The data for outcome variables were obtained through chart review and confirming with patient/patient family phone calls. Each patient/patient family was attempted to be contacted 3 times if they did not initially answer.

Follow-up was obtained through the electronic medical record, or, in cases of > 6 months of missing follow-up data, phone calls to patients and/or patients’ designated healthcare advocates.

Other covariates of interest:

Patient charts were reviewed for patient demographics, including age at surgery (difference between initial surgery date and date of birth), biological sex, race (white, African American, Latinx, Asian, or other), body mass index (BMI, kg/m^2), Karnofsky Performance Status (KPS)[52], and preoperative comorbidities (see above). Preoperative neurological status was assessed by

report of seizures, presence of neurological deficit. Postoperative neurological status was assessed by presence of a neurological deficit, seizures after surgery (during hospitalization), KPS at discharge, and Modified Rankin Scale (mRS) at discharge.[53] Postoperative complications included presence of hemorrhage, surgical site infection, length of stay, or other medical complication (including non-surgical site infection, deep vein thrombosis, or cardiopulmonary event). Data about surgical procedures included if the lesion was recurrent, i.e. operated upon at another institution prior to our care. In these cases, the date of the initial surgery was recorded. Other surgical data included whether the patient received a stereotactic needle biopsy, or craniotomy for resection, and date of surgery (as well as subsequent surgeries at one of our institutions). Post-hospitalization covariates included whether the patient received adjuvant chemotherapy or chemotherapy, discharge disposition (home, rehabilitation center, long-term acute care center).

All patients included in the study had genetic analysis completed to confirm histopathological diagnosis. Glioma tissue obtained through surgery is examined with immunohistochemistry, cytogenomic DNA copy number microarray (OncoScan® -Thermo Fisher Scientific), multiplex PCR (SNaPshot™ - Thermo Fisher Scientific) with MetaCore™ (Clarivate Analytics) enrichment for identification of associated molecular pathways.

Statistical analysis:

Statistical analyses were performed using R Statistical Software (version 4.1.1, R Foundation for Statistical Computing, Vienna, Austria) and SAS version 9.4 (SAS Institute, Cary, NC). We

described the cohort characteristics by frailty status (i.e., high or low) dichotomized all variables were assessed for normality; means were reported when variables were distributed normally and medians/interquartile ranges were reported when otherwise. To assess the association between frailty and 30-day readmission, we conducted an unadjusted logistic regression. A directed acyclic graph (DAG—see **Figure 3**) was used to our multivariable-adjsuted model. We assessed the association between frailty and 30-day readmission both for frailty and CCI indices. For the logistic regression models, we reported odds ratios (OR) and adjusted ORs (aOR) with 95% confidence intervals (CI).

Overall survival was assessed with cumulative Kaplan-Meier survival curves and cox-proportional hazard models to evaluate whether the mFI-5 or CCI frailty exposure was associated with the rate of overall survival. We dichotomized survival curves by surgery type (biopsy vs. resection surgery), tumor genetic lineage (astrocytoma vs. oligodendroglioma), and primary tumor location (cortically-based/lobar vs. deep brain structure). Censorship was defined as above (Outcomes). Proportional hazard assumptions for covariates were assessed graphically, with goodness-of-fit tests, and time-dependent models. Similar to the process completed for assessment of variables to include in our logistic models, we used bivariate associations between frailty exposure and OS outcome as well as a DAG to inform our Cox-proportional hazards model (**Figure 3**). For the Cox-proportional hazards model, we reported hazard ratios (HR), adjusted HRs (aHR), and 95% CIs. Missing data for each covariate of interest can be found in **Table 1**.

Aim 1 and hypotheses:

The primary aim of this study was to examine the association between frailty (measured by two frailty metric scores) and 30-day readmission in patients undergoing biopsy or surgical resection of *IDH*-mutant glioma. Our secondary aim was to study the effect of frailty on overall survival in the same surgical population of patients with *IDH*-mutant glioma. We hypothesize that (1) higher level of frailty would be associated with an increased risk for 30-day readmission, and (2) that higher level of frailty would be associated with shorter overall survival.

Aim 2 Methods: Copy number (CN) variations and *IDH*-mutant gliomas

Variables:

Main exposure:

CN variation quantifies the number of point mutations in a tumor sample. It provides an estimation of the mutational burden within a tumor and has been related to overall survival (OS) and progression free survival (PFS) in different glioma types. Total CN variation was collected using glioma tissue that underwent cytogenomic DNA copy number microarray (OncoScan® - Thermo Fisher Scientific), multiplex PCR (SNaPshot™ - Thermo Fisher Scientific) with MetaCore™ (Clarivate Analytics) enrichment. Total CN variation was completed with adding the total number of gains of nucleotides, deletions, and losses of heterozygosity.

Other covariates of interest:

Output of the genetic microarray analysis provides which specific chromosomes feature gains, deletions, or losses of heterozygosity. For each patient, these were collected for the secondary analysis. Please see above section for other covariates collected in the *IDH*-mutant database.

Statistical analysis:

Descriptive statistics were reported using median with range for numeric variables and frequency and percentage for categorical covariates. The total CNV variable was dichotomized using different approaches: Median, quartiles and optimal cut point (https://molpathoheidelberg.shinyapps.io/CutoffFinder_v1/). PFS was defined from diagnosis to death or progression whichever came earlier or last follow up for those censored. PFS was estimated using the Kaplan-Meier method and compared using log-rank tests. OS was defined from diagnosis to death for those with event or last follow up for those censored. % Total CNV was calculated by dividing each samples value by the total and multiplying by 100. Correlation between % Total CNV and overall survival time was estimated using Pearson correlation coefficient and the correlation test p-value was reported. Similarly, correlation between % Total CNV and progression free survival time was also reported.

Copy segment values were converted into binary matrix based on whether a patient has an amplification or deletion (1) vs not (0). Data was scaled using a modified z-score for columns (samples). Heatmap were created using Manhattan distance and ward.D agglomerative clustering using NOJAH tool. OS and PFS based on column clusters were reported with a log rank test to evaluate if the samples differ based on clustering. Alternately, copy segment values were

converted into a matrix based on whether a patient has an amplification (1) or deletion or loss of heterozygosity (-1) vs not (0). Heatmap was created using manhattan distance and ward.D agglomerative clustering and OS and PFS between clusters were compared similar to above.

Statistical analysis was performed using SAS 9.4 (SAS Institute Inc., Cary, NC) macros, and heatmaps were generated using NOJAH and statistical significance was assessed at the 0.05 level.[54,55]

Aim 2 and hypotheses:

The primary aim of this study was to examine the association between CNV and PFS and OS. Our secondary aim was to run a heat map analysis to find if specific chromosomal mutations related to OS or PFS. Our hypothesis was that CNV would relate to OS and PFS and that higher CNV total would portend a lower OS and PFS.

Aim 3 Methods: Radiographic parameters

Data collection and preprocessing:

Images from the *IDH*-mutant database were ascertained by downloading pre-operative and post-operative images from the picture archiving and communication system (PACS) by patient accession number. A patient had complete imaging if they had stereotactic-quality, T1-weighted (T1W) post-gadolinium contrast MRI pre- and post-operative images (1.5 Tesla MRI with at least <1.25 mm slice thickness) Images were reviewed and confirmed to be pre-surgical and

found to be high quality with appropriate resolution. Any images with artifact or substantial noise were excluded from analyses. The dataset was preprocessed to ensure uniformity and quality, which included conversion to .nifti imaging format. Bias field correction was performed. Skull stripping utilizing HD-BET.[56] Further preprocessing included cropping, resizing images (128xc128x128), normalizing intensity values, and correcting for artifacts or noise using TorchIO.[57]

Data augmentation:

To improve the performance and generalizability of the model, data standard augmentation techniques were employed to increase the size and diversity of the dataset. This included random application of affine transformations, flips, and rotations of the images, as well as adding small elastic deformations or other distortions. This was perfomed using the TorchIO.

Model Selection:

Choosing the appropriate deep learning model architecture is crucial for achieving accurate predictions. Several models have been shown to be effective for binary classification, including Convolutional Neural Networks (CNNs), and Recurrent Neural Networks (RNNs). This study employed a 3D residual neural network (ResNet18) model given the desire to use MRI imaging to train to identify pathological subtype. The decided outcome of the model was the tumor lineage, oligodendroglioma or astrocytoma (**Figure 1**).

We also planned to create a dense-neural network using binary, categorical, and continuous variables for the same outcome, to compare the efficacy of the MR imaging-only model. Variables that we included were: presence of preoperative seizure (yes/no), presence of preoperative neurological deficit (yes/no), whether the tumor was identified incidentally (yes/no), whether the tumor was in eloquent brain matter [speech, motor, visual center, brainstem] (yes/no), sex (male/female), race (white, black, Asian, latinx, other), KPS, tumor location (frontal, temporal, parietal, occipital, insula, cerebellum), contrast type (full enhancement, heterogenous, none). We planned for a local Bayesian search to design the network and optimize hyperparameters. We planned to standardize the data, perform Tanh activation function, and form a dense neural network.

Training the Models:

The deep-learning imaging-only model was trained on the preprocessed dataset and augmentation was performed using a data loader in real time. This involves dividing the dataset into training (85%), and validation (15%) sets using binary focal cross entropy loss function to optimize the model's weights and biases. 150 epochs were performed to complete the training process with an Adam optimization with decaying learning rate.

The deep-learning, non-imaging model was trained on 150 epochs.

Hyperparameter Tuning:

The performance of the model can be further improved by tuning its hyperparameters, such as learning rate, batch size, and regularization strength. This was performed using random search, to find the optimal set of hyperparameters that maximize the model's accuracy and minimize loss.

Evaluation:

Once the model was trained and tuned, metrics such as accuracy, precision, recall, and F1 score can be used to evaluate the model's performance on each class. All models were generated Keras/Tensorflow within the Python language with standard libraries.

Results:

Query of our database included 136 patients with *IDH*-mutant glioma (**Table 1**). Forty-nine (49, 36%) patients had oligodendroglioma, while 87 (64%) had astrocytoma. Overall, 87 (64%) patients underwent attempted surgical resection, while 49 (36%) had an open or stereotactic needle biopsy.

Aim 1 Results:

Eighteen (18, 13%) of patients had a CCI greater than or equal to 3 (“high CCI”), while 34 (25%) of patients had a mFI-5 greater than or equal to 1 (“high mFI-5”) (**Table 1**). Patients with

high frailty scores had high body mass index (BMI) (CCI: 30.2 kg/m^2 [Interquartile Range/IQR: 24.4 - 37.0 kg/m^2]; mFI-5: 30.1 kg/m^2 [IQR: 23.4 – 34.4]), more preoperative neurological deficit (CCI: 11/18, 61%; mFI-5: 19/34, 56%), and older age at surgery (CCI: 63 years [IQR: 56 – 73 years]; mFI-5: 48 years [IQR: 39 – 62 years]). The total mutational burden of the tumor, measured by CN variation, was relatively equal among those with high and low frailty

Eight (8, 5.9%) of patients experienced the primary outcome of hospital readmission within 30 days of surgery. The OS for the entire cohort is displayed in **Figure 4**. The median survival length was 54 months. When divided into groups with high and low frailty, patients with higher frailty seemed to have lower OS probability, though the curves did cross (**Figure 5**).

In our logistic regression for the outcome of odds of 30-day readmission, the crude odds of 30 day readmission in patients with high CCI was 0.93 (0.04 – 5.72) times that of those that had a low CCI. In the adjusted logistic regression, the odds of 30 day readmission in patients with high CCI was 0.22 (0.01 – 3.24), adjusting for tumor location, BMI, type of surgery, and age (**Table 2)**. The crude odds of 30 day readmission in patients with high mFI-5 was 1.88 (0.37 – 8.10) times that of those that had a low mFI-5. In the adjusted logistic regression, the odds of 30 day readmission in patients with high mFI-5 was 1.56 (0.24 – 8.96), adjusting for tumor location, BMI, type of surgery, and age (**Table 2)**.

The median survival time of patients with high CCI (11.1 months [IQR: 1.1 – 58.0 months]) were lower than those with low CCI (55.3 months [IQR: 22.0 – 99.1 months]), however, the IQRs overlapped. The median survival time of patients with high mFI-5 (26.3 months [IQR: 2.5

– 55.3 months]) were lower than those with low mFI-5 (63.1 months [IQR: 31.6 – 99.8 months]), again, the IQRs overlapped (**Table 3**).

In our Cox-proportional hazards analysis, the crude hazard rate of death in patients with high CCI was 3.33 (1.12 – 9.97) times the hazard rate of death in patients with low CCI (**Table 3**). In the adjusted analysis, the adjusted hazard rate of death in patients with high CCI was 0.59 (0.05 – 6.37) times the hazard rate of death in patients with low CCI, adjusting for age, tumor location, BMI, history of prior surgery, and type of surgery. Using our other frailty metric, the crude hazard rate of death in patients with high mFI-5 was 2.14 (0.83 – 5.47) times the hazard rate of death in patients with low mFI-5 (**Table 3**). In the adjusted analysis, the adjusted hazard rate of death in patients with high mFI-5 was 1.15 (0.29 – 4.52) times the hazard rate of death in patients with low mFI-5, adjusting for age, tumor location, BMI, history of prior surgery, and type of surgery.

When we subdivided the cohort into patients that had biopsy vs. craniotomy for resection and into astrocytoma vs. oligodendroglioma lineage, we found that there was no significant separation of survival curves (**Figure 6**).

When we subdivided the cohort by patients who had new tumor diagnoses and first operated upon at our institution (i.e. excluding recurrent tumors), we found that the adjusted hazard ratio of death in patients with high mFI-5 was 6.79 (1.00 – 45.9) times that of the adjusted hazard ratio of death in patients with low mFI-5, when adjusting for age, tumor location, BMI, and surgery type (**Table 4)**.

Aim 2 Results:

A total of 88 patients had complete pathology data for the CN variation and heatmap analysis (**Table 5**). The mean number of CN variations was 12.8 (standard deviation, SD: 11.36), and the median was 8.5 (IQR: 5 – 17.5). The ideal cutpoint calculator (https://molpathoheidelberg.shinyapps.io/CutoffFinder_v1/), defined a CN variation of 10.5 for OS analysis and 7.5 for PFS analysis.

In our Kaplan-Meier survival analysis for PFS, when dividing the cohort by CN variation median, we found that median survival for patients with total CN variation <= 8.5 was 10.5 years (95% confidence interval, CI: 4.2 – 16 yrs), while the median survival for patients with total CN variation > 8.5 was 6.6 years (95% CI: 2.4 – 8.3 yrs), [logrank p-value: 0.085] (**Figure 7A**). **Figure 7B** displays the results of performing the analysis after subdividing the cohort into quartiles (logrank p-value: 0.16). In the optimal cutpoint analysis, patients that had a total CN variation <= 7.5 had a median survival of 10.3 years (95% CI: 4.2 – 29.8 yrs), while patients that featured a total CN variation >7.5 had a median survival of 4.6 years (95% CI: 2.4 – 8.3 yrs). The separation of the survival curves using optimal cutpoint for total CN variation was statistically significant, as logrank p-value = 0.042.

Next, we applied our Kaplan-Meier survival analysis for OS. When halving our cohort by the CN variation median, we found that the median survival with CN variation <= 8.5 was 29.8 years (95% CI: infinite – infinite), and incalculable for the CN variation >8.5. The logrank p-

value was 0.20 (**Figure 8A**). We split the cohort by CN variation quartile and found logrank p-vaule to be 0.042 (**Figure 8B**). When repeating the Kaplan-Meier survival analysis by optimal cutpoint, we found that CN variation <= 10.5 had median survival of 29.8 yrs (95% CI: infinite – infinite) and CN variation > 10.5 was incalculable; logrank p-value = 0.067 (**Figure 8C**).

In **Figure 9A** and **9B**, we attempted to recapitulate a correlation analysis completed in Mirchia et al. 2019, wherein the authors were able to describe an inverse correlation of total CN variation and OS. We found the Spearman-rho correlation to be close to 0; 0.011 for OS (p-value= 0.92) and 0.005 for PFS (p-value= 0.97).

We performed two heatmap analyses to find clusters of patients with different OS and PFS within this cohort. In the first heatmap analysis, events were coded "1" for chromosomal amplification or deletion, and "0" for no change from normal (**Figure 10A**). We performed Kaplan-Meier survival analysis for the outcomes of OS and PFS comparing the hierarchical clusters formed by this analysis. In **Figure 10B**, cluster 1 had a median OS of 6 years (95% CI: 3.6 – 9.5 years), while cluster 2 had median OS of 8.3 years (95% CI: 0.3 – infinite years) (logrank p-value= 0.38). In **Figure 10C**, we compared these clusters in PFS. Cluster 1 had median survival of 29.8 years (95% CI: 10 – 29.8 years), while cluster 2 had an incalculable median survival (logrank p-value= 0.50).

In the second heatmap analysis, we coded "1" as a chromosomal gain, "0" as no change, and "-1" as chromosomal deletion or loss of heterozygosity. **Figure 11A** displays the heatmap analysis output. In PFS survival analysis (**Figure 11B**), cluster 1 had a median PFS of 7.3 years (95% CI:

4.2 – 9.5 years), while cluster 2 had a median PFS of 8.3 years (0.4 – infinite years) (logrank p-value= 0.56). In OS survival analysis (**Figure 11C**), the median OS for cluster 1 was 29.8 years (95% CI: 10 - 29.8 years), while median OS for cluster 2 was incalculable (logrank p-value= 0.90).

Aim 3 Results

Non-imaging-based deep-learning model:

First, we created a simple deep learning model to predict pathological subtype during the preoperative evaluation which would be imaging naive. Using 135 patients, 126 of who had complete preoperative information, we trained a fully connected neural network with TanH activation function and tuned hyperparameters using local Bayesian search. The data was split into 85% training cohort and 15 % validation cohort. We then evaluated the cohorts using various metrics. The model parameters included demographic information: gender, race, and age, and clinical data: KPS at presentation, tumor location, tumor side, contrast enhancement type, history of seizure, presence of preoperative neurological deficit, whether the tumor was an incidental discovery, and eloquent location.

Evaluation of or model resulted in a validation set performance of 77.8% accuracy with AUC of 0.8667. Our training set performance was 75.93% accurate with AUC of 0.8169.

MR imaging-based deep-learning model:

We then trained an imaging-only model to identify predict oligodendroglioma subtype vs astrocytoma subtype of *IDH*-mutant gliomas. Using methods described above we trained a 3D ResNet18 on preoperative T1W post-contrast MR images. Images were manually reviewed and preoprocessed as detailed in methods. The dataset was divided into a training and validation cohort (85%/15% (n= 87/16)). The 3D ResNet18 was trained for 150 epochs (**Figure** .

Overall, the training accuracy of our model was 93.75%, AUC 0.9788, [TP28, FP2, TN47, FN3] F1-Score 0.9180 (**Table 6**). The validation accuracy for our model was 81.25%, AUC 0.9091, [TP4, FP2, TN9, FN1], F1-Score 0.7273 (**Table 7**).

Discussion:

Aim 1:

In this aim, we described the relation of the exposure of frailty (measured by two metrics) upon two outcomes; 30-day readmission and OS. We found that CCI and mFI-5 were not associated with 30-day readmission. We also found that CCI and mFI-5 were not associated with OS. However, in patients that had their first surgery at our institution (not recurrent tumors), there was an association of one frailty measure (mFI-5) with OS.

While we hypothesized that frailty would be associated with 30-day readmission and OS in our cohort, there are multiple reasons why we may have not discovered such associations. While our single-institution experience of *IDH*-mutant glioma is relatively large, the overall small sample size (n = 136) and resulting under-powered statistical analyses did not allow for effective testing of true associations. In short, our study is marred by type II error.

Additionally, the proportion of patients with high frailty in our cohort is small, with only 13.2% (n = 18) of patients having high CCI and 25% (n=34) of patients having high mFI-5. Overall, patients with *IDH*-mutant glioma tend to be younger, and thus more healthy/less frail than other brain tumor cohorts (**Table 1**).[43] Patients with metastatic tumors tend to be older and have more systemic disease than patients with *IDH*-mutant glioma we studied in our cohort and others.[58,59] The event rate of 30-day readmission in the cohort was low as well (5.9%, n = 8). These limitations reduce the ability to detect associations between frailty and our primary outcome.

There are other factors that may explain the lack of association of frailty with outcome in patients with glioma. The type of surgery that patients receive has significant association with readmission, PFS, and OS. While still somewhat controversial, it is generally accepted that patients with glioma that obtain a maximal safe surgical resection have increased time to recurrence and mortality.[44,60–62] However, the association of extent of resection and outcome is plagued by numerous confounders. For example, there is significant bias in the administration of attempted gross total resection; neurosurgeons will not attempt aggressive resection in tumors located in eloquent areas of the brain or in older patients or patients that have significant medical comorbidities.[32,62] Additionally, tumor genetics play a larger role in outcome in patients with glioma compared to other lesions of the brain. Patients with HGG have shorter OS and PFS than patients with LGG.[2,4,12,14,43] Surgery type, extent of resection, and genetic factors are examples of parameters that play a role in outcome of patients with glioma and may disrupt associations of frailty and outcome in glioma cohorts.

Other groups have described the association of frailty with OS in patients with brain tumors. Youngerman et al. found that the modified frailty index was associated with 30-day readmission, mortality, medical complications, neurological complications, prolonged length of stay, and discharge to rehabilitation facility rather than home.[33] There are major differences in the *IDH*-mutant glioma cohort and the cohort used for the Youngerman et al. study. First, the data to form the cohort in the Youngerman et al. study were from the American College of Surgeons NSQIP database, and had a much larger sample size (n=9149 patients). This cohort was more adequately powered to discover the associations delineated above. Second, fewer than one-half of patients in

the NSQIP database had glioma. Third, the cohort had a greater percentage of patients with frailty, with 48.5% having at least low frailty.

Cloney et al. and Khalafallah et al. also related frailty measures to outcome in patients with brain tumors.[32,63] Cloney et al. studied the exposure of frailty within a cohort of 319 geriatric patients with HGG. They found that patients with more frailty were less likely to undergo surgical resection (vs. biopsy), had longer stay in hospital, and increased overall risk of complications. Differences in this cohort compared to our *IDH*-mutant cohort is the older age of patients, higher rates of frailty, and more homogenous tumor type (HGG). Khalafallah et al. described the relationship of frailty and outcome in 1692 patients with brain tumors. They found that increased frailty related to 90-day mortality, in a dose-adjusted pattern. Key differences in this cohort to ours include increased sample size, low rate of glioma diagnosis (<30%), and very low rate of outcome of mortality (3%).

In future studies with this cohort, we could strengthen our ability to test associations between frailty and outcome in *IDH*-mutant glioma by increasing sample size, testing different levels of the exposure (different cut off points for "high" vs. "low" frailty), and including sensitivity analyses. Additionally, we could implement Bayesian analytic strategies to analyze this low sample size database.[64]

<u>Aim 2:</u>

Using next-generation molecular/genetic sequencing of *IDH*-mutant glioma tissue, we attempted to discover associations between CN variation and outcomes of OS and PFS within our cohort. We also performed a heat-map analysis to find clusters of genotypes that relate to the outcomes of OS and PFS.

Overall, our results suggest that there may be an association with increased CN variation and PFS. Using an optimized cut-point, there was a significant negative difference in survival in patients with higher CN variation than those with lower CN variation in our cohort (**Figure 7**). The Kaplan-Meier curves (**Figures 7 and 8**) show separation when comparing high CN variation vs. low CN variation median as cut-point for PFS and OS. While the logrank p-values were only significant for the Kaplan-Meier curves when we employed optimized cut-point, the separation in the curves suggest that with larger sample size, the ability to detect an association may be greater. Our heat-map analysis did not discover a clusters with differing PFS nor OS.

There are multiple issues with our database that reduce the likelihood of finding meaningful associations between genetic factors and outcomes in *IDH*-mutant glioma. Again, while we have a relatively expansive single-institution experience in *IDH*-mutant glioma, our overall sample size is likely too small to detect differences between patients, especially when performing high-dimensional data analysis (heat-map). Our results of the overall survival analysis are marred by high rate of censorship and low event rate of observed death. The observed rate of death amongst patients with complete next-generation sequencing analysis was 11.4% (**Figures 7 and 8**). While we attempted to contact patient families for updated survival data, we suffered from a significant number of patients being lost to follow-up.

Mirchia et al. studied the prognostic capability of CN variations within *IDH*-mutant and *IDH*-wildtype gliomas.[23] They further subdivided *IDH*-mutant tumors as those with *CDKN2A/B* deletion or *CDK4* amplification, those without, and *IDH*-mutant HGG. Their data suggested that increased CN variation number was predictive of prognosis in patients with *IDH*-mutant tumors, but not in patients with *IDH*-wildtype tumors. The analytic approach of the Mirchia et al. paper was different than ours. They subdivided the *IDH*-mutant heterogenous groups into more homogenous patient cohorts by previously-described biomarkers (*CDKN2A/B* and *CDK4*). This allowed for cleaner statistical output, however, potentially lowers the generalizability of their findings. While the main findings of the article report that CN variation is a prognostic parameter in patients with *IDH*-mutant glioma, the reality is that the associations are restricted to specific *IDH*-mutant groups, and less generalizable.

Buchwald et al. studied the association of CN variations in 56 patients with HGG (WHO grade IV glioblastoma), and externally-validated their findings using the Cancer Genome Atlas (TCGA).[65] Contradictory to ours and Mirchia et al. reports, Buchwald et al. found that increased CN variation was associated with increased PFS and OS. The findings in this study run in conflict to other cancer types and *IDH*-mutant glioma, where increased CN variation seems to correlate with decreased PFS and OS.[23,66–68]

In future analyses with this dataset, we would like to increase our sample size by adding patients with complete genetic data. We could also improve our follow-up to receive more event data for PFS and OS analyses. Another future study could include subdividing our cohort by known

prognostic mutations (such as *CDKN2A/B* and *CDK4*), to recapitulate the analysis completed by Mirchia et al. Last, we could externally validate our analysis on shared databases such as the TCGA.

Aim 3:

In this aim of the project, we developed two algorithms using machine-learning/deep-learning adaptive neural networks to predict the outcome of tumor lineage: astrocytoma or oligodendroglioma. The non-imaging-based predictive model had a training performance accuracy of 75.9% and AUC of 0.82, while the validation performance accuracy was 77.8% and the AUC was 0.87. The imaging-based predictive model had a training performance accuracy of 93.8% and AUC of 0.98, while the validation performance accuracy was 81.3% with AUC 0.91 (**Table 6 and 7**).

Others have used MRI parameters to help predict tumor type and outcomes in the glioma patient population. Bumes et al. employed PET-guided MR spectroscopy images and machine-learning analysis to predict whether or not a glioma patient harbored an *IDH*-mutation.[69] Others have attempted to predict *IDH* mutation status amongst patients with gliomas.[70,71] To our knowledge, our analysis is the first attempt to discover *IDH*-mutant glioma genomic lineage with an imaging-based, machine-learning algorithm.

Having a tool to predict tumor lineage could assist neurosurgeons in the care of patients with suspected *IDH*-mutant glioma. Recent analyses suggest that attempted gross total resection may

confer an OS and PFS benefit to *IDH*-mutant astrocytoma, but not for oligodendroglioma.[72] While the conclusions from such studies should be accepted with caution owing to their class III/IV evidence standing, preoperative identification of tumor lineage could prove to be helpful to neurosurgeons and oncologists. Surgery has the potential for more risk than most neurosurgeons care to admit. For example, the late term neurocognitive side effects of attempted aggressive resection could be underappreciated.[73,74]

Our model for predicting tumor lineage is nascent. Moving forward, we aim to improve the predictive capacity of this algorithm by combining non-imaging based and MRI-based parameters together. We want to use more imaging modalities, such as T2W MRI sequences, diffusion-tensor, and diffusion weighted imaging to strengthen our algorithm. Additionally, we could increase sample size by adding patients to our database and using externally-maintained data repositories such as the TCGA. We would also like to apply the techniques in this study to predict different outcomes, such as PFS and OS.

References

1. Parsons DW, Jones S, Zhang X, et al. An integrated genomic analysis of human glioblastoma multiforme. *Science*. 2008;321(5897):1807-1812. doi:10.1126/science.1164382

2. Eckel-Passow JE, Lachance DH, Molinaro AM, et al. Glioma groups based on 1p/19q, IDH, and TERT promoter mutations in tumors. *New England Journal of Medicine*. 2015;372(26):2499-2508. doi:10.1056/NEJMoa1407279

3. Louis DN, Perry A, Burger P, et al. International Society Of Neuropathology--Haarlem consensus guidelines for nervous system tumor classification and grading. *Brain pathology (Zurich, Switzerland)*. 2014;24(5):429-435. doi:10.1111/bpa.12171

4. Louis DN, Perry A, Reifenberger G, et al. The 2016 World Health Organization Classification of Tumors of the Central Nervous System: a summary. *Acta Neuropathologica*. 2016;131(6):803-820. doi:10.1007/s00401-016-1545-1

5. Wang Y, Jiang T. Understanding high grade glioma: Molecular mechanism, therapy and comprehensive management. *Cancer Letters*. 2013;331(2):139-146. doi:10.1016/j.canlet.2012.12.024

6. Noiphithak R, Veerasarn K. Clinical predictors for survival and treatment outcome of high-grade glioma in Prasat Neurological Institute. *Asian journal of neurosurgery*. 2017;12(1):28-33. doi:10.4103/1793-5482.148791

7. Riemenschneider MJ, Jeuken JWM, Wesseling P, Reifenberger G. Molecular diagnostics of gliomas: State of the art. *Acta Neuropathologica*. 2010;120(5):567-584. doi:10.1007/s00401-010-0736-4

8. Nduom EK, Wei J, Yaghi NK, et al. PD-L1 expression and prognostic impact in glioblastoma. *Neuro-Oncology*. 2016;18(2):195-205. doi:10.1093/neuonc/nov172

9. Heimberger AB, Abou-Ghazal M, Reina-Ortiz C, et al. Incidence and Prognostic Impact of FoxP3⁺ Regulatory T Cells in Human Gliomas. *Clinical Cancer Research*. 2008;14(16):5166 LP - 5172. doi:10.1158/1078-0432.CCR-08-0320

10. Masui K, Mischel PS, Reifenberger G. *Molecular Classification of Gliomas*. Vol 134. Elsevier B.V.; 2016. doi:10.1016/B978-0-12-802997-8.00006-2

11. Geng RX, Li N, Xu Y, et al. Identification of core biomarkers associated with outcome in glioma: Evidence from bioinformatics analysis. *Disease Markers*. 2018;2018. doi:10.1155/2018/3215958

12. Yan H, Parsons DW, Jin G, et al. IDH1 and IDH2 Mutations in Gliomas. *New England Journal of Medicine*. 2009;360(8):765-773. doi:10.1056/NEJMoa0808710

13. Sanson M, Marie Y, Paris S, et al. Isocitrate Dehydrogenase 1 Codon 132 Mutation Is an Important Prognostic Biomarker in Gliomas. *Journal of Clinical Oncology*. 2009;27(25):4150-4154. doi:10.1200/JCO.2009.21.9832

14. Brat DJ, Verhaak RGW, Aldape K. Comprehensive, Integrative Genomic Analysis of Diffuse Lower-Grade Gliomas. *https://doi.org/101056/NEJMoa1402121*. Published online June 18, 2015. https://www.nejm.org/doi/10.1056/NEJMoa1402121

15. Reuss DE, Sahm F, Schrimpf D, et al. ATRX and IDH1-R132H immunohistochemistry with subsequent copy number analysis and IDH sequencing as a basis for an "integrated" diagnostic approach for adult astrocytoma, oligodendroglioma and glioblastoma. *Acta Neuropathologica*. 2015;129(1):133-146. doi:10.1007/s00401-014-1370-3

16. Hattori N, Hirose Y, Sasaki H, et al. World Health Organization grade II-III astrocytomas consist of genetically distinct tumor lineages. *Cancer Science*. 2016;107(8):1159-1164. doi:10.1111/cas.12969

17. Pekmezci M, Rice T, Molinaro AM, et al. Adult infiltrating gliomas with WHO 2016 integrated diagnosis: additional prognostic roles of ATRX and TERT. *Acta Neuropathologica*. 2017;133(6):1001-1016. doi:10.1007/s00401-017-1690-1

18. Reuss DE, Mamatjan Y, Schrimpf D, et al. IDH mutant diffuse and anaplastic astrocytomas have similar age at presentation and little difference in survival: a grading problem for WHO. *Acta Neuropathologica*. 2015;129(6):867-873. doi:10.1007/s00401-015-1438-8

19. Hegi ME, Diserens AC, Gorlia T, et al. MGMT Gene Silencing and Benefit from Temozolomide in Glioblastoma. *New England Journal of Medicine*. 2005;352(10):997-1003. doi:10.1056/nejmoa043331

20. Reis GF, Pekmezci M, Hansen HM, et al. CDKN2A loss is associated with shortened overall survival in lower-grade (World Health Organization Grades II-III) astrocytomas. *Journal of Neuropathology and Experimental Neurology*. 2015;74(5):442-452. doi:10.1097/NEN.0000000000000188

21. Aoki K, Nakamura H, Suzuki H, et al. Prognostic relevance of genetic alterations in diffuse lower-grade gliomas. *Neuro-Oncology*. 2018;20(1):66-77. doi:10.1093/neuonc/nox132

22. Zhou X, Li G, An S, et al. A new method of identifying glioblastoma subtypes and creation of corresponding animal models. *Oncogene*. 2018;37(35):4781-4791. doi:10.1038/s41388-018-0305-1

23. Mirchia K, Sathe AA, Walker JM, et al. Total copy number variation as a prognostic factor in adult astrocytoma subtypes. *Acta Neuropathologica Communications*. 2019;7(1):92. doi:10.1186/s40478-019-0746-y

24. Richardson TE, Snuderl M, Serrano J, et al. Rapid progression to glioblastoma in a subset of IDH-mutated astrocytomas: a genome-wide analysis. *Journal of Neuro-Oncology*. 2017;133(1):183-192. doi:10.1007/s11060-017-2431-y

25. Richardson TE, Sathe AA, Kanchwala M, et al. Genetic and Epigenetic Features of Rapidly Progressing IDH-Mutant Astrocytomas. *Journal of Neuropathology and Experimental Neurology*. 2018;77(7):542-548. doi:10.1093/jnen/nly026

26. Nakae S, Kato T, Murayama K, et al. Remote intracranial recurrence of IDH mutant gliomas is associated with TP53 mutations and an 8q gain. *Oncotarget*. 2017;8(49):84729-84742. doi:10.18632/oncotarget.20951

27. Boots-Sprenger SHE, Sijben A, Rijntjes J, et al. Significance of complete 1p/19q co-deletion, IDH1 mutation and MGMT promoter methylation in gliomas: use with caution. *Modern Pathology*. 2013;26(7):922-929. doi:10.1038/modpathol.2012.166

28. Ortman JM, Velkoff V a., Hogan H. An aging nation: The older population in the United States. *Economics and Statistics Administration, US Department of Commerce*. 2014;1964:1-28.

29. Vaupel JW, Manton KG, Stallard E. The impact of heterogeneity in individual frailty on the dynamics of mortality. *Demography*. 1979;16(3):439-454.

30. Karam J, Tsiouris A, Shepard A, Velanovich V, Rubinfeld I. Simplified frailty index to predict adverse outcomes and mortality in vascular surgery patients. *Annals of Vascular Surgery*. 2013;27(7):904-908. doi:10.1016/j.avsg.2012.09.015

31. Clegg A, Young J, Iliffe S, Rikkert MO, Rockwood K. Frailty in elderly people. *The Lancet*. 2013;381(9868):752-762. doi:https://doi.org/10.1016/S0140-6736(12)62167-9

32. Cloney M, D'Amico R, Lebovic J, et al. Frailty in Geriatric Glioblastoma Patients: A Predictor of Operative Morbidity and Outcome. *World Neurosurgery*. 2016;89:362-367. doi:10.1016/j.wneu.2015.12.096

33. Youngerman BE, Neugut AI, Yang J, Hershman DL, Wright JD, Bruce JN. The modified frailty index and 30-day adverse events in oncologic neurosurgery. *Journal of Neuro-Oncology*. 2018;136(1):197-206. doi:10.1007/s11060-017-2644-0

34. Huq S, Khalafallah AM, Jimenez AE, et al. Predicting Postoperative Outcomes in Brain Tumor Patients With a 5-Factor Modified Frailty Index. *Neurosurgery*. 2020;88(1):147-154. doi:10.1093/neuros/nyaa335

35. Shirahata M, Ono T, Stichel D, et al. Novel, improved grading system(s) for IDH-mutant astrocytic gliomas. *Acta Neuropathologica*. 2018;136(1):153-166. doi:10.1007/s00401-018-1849-4

36. Yoda RA, Marxen T, Longo L, et al. Mitotic Index Thresholds Do Not Predict Clinical Outcome for IDH-Mutant Astrocytoma. *Journal of Neuropathology and Experimental Neurology*. 2019;78(11):1002-1010. doi:10.1093/jnen/nlz082

37. Brat DJ, Aldape K, Colman H, et al. cIMPACT-NOW update 5: recommended grading criteria and terminologies for IDH-mutant astrocytomas. *Acta Neuropathologica*. 2020;139(3):603-608. doi:10.1007/s00401-020-02127-9

38. Kumar V, Gu Y, Basu S, et al. Radiomics: the process and the challenges. *Magnetic resonance imaging*. 2012;30(9):1234-1248. doi:10.1016/j.mri.2012.06.010

39. Lehrer M, Rao A, Bhadra A, et al. Multiple-response regression analysis links magnetic resonance imaging features to de-regulated protein expression and pathway activity in lower grade glioma. *Oncoscience*. 2017;4(5-6):57-66. doi:10.18632/oncoscience.353

40. Gutman DA, Cooper LAD, Hwang SN, et al. MR imaging predictors of molecular profile and survival: Multi-institutional study of the TCGA glioblastoma data set. *Radiology*. 2013;267(2):560-569. doi:10.1148/radiol.13120118

41. Panth KM, Leijenaar RTH, Carvalho S, et al. Is there a causal relationship between genetic changes and radiomics-based image features? An in vivo preclinical experiment with doxycycline inducible GADD34 tumor cells. *Radiotherapy and Oncology*. 2015;116(3):462-466. doi:https://doi.org/10.1016/j.radonc.2015.06.013

42. Castet F, Alanya E, Vidal N, et al. Contrast-enhancement in supratentorial low-grade gliomas: a classic prognostic factor in the molecular age. *Journal of Neuro-Oncology*. 2019;143(3):515-523. doi:10.1007/s11060-019-03183-2

43. Miller JJ, Gonzalez Castro LN, McBrayer S, et al. Isocitrate dehydrogenase (IDH) mutant gliomas: A Society for Neuro-Oncology (SNO) consensus review on diagnosis, management, and future directions. *Neuro-Oncology*. 2022;25(1):4-25. doi:10.1093/neuonc/noac207

44. Jiang B, Chaichana K, Veeravagu A, Chang SD, Black KL, Patil CG. Biopsy versus resection for the management of low-grade gliomas. Cochrane Gynaecological, Neuro-oncology and Orphan Cancer Group, ed. *Cochrane Database of Systematic Reviews*. 2017;2020(6). doi:10.1002/14651858.CD009319.pub3

45. Subramaniam S, Aalberg JJ, Soriano RP, Divino CM. New 5-factor modified frailty index using American College of Surgeons NSQIP data. *Journal of the American College of Surgeons*. 2018;226(2):173-181.

46. Charlson ME, Pompei P, Ales KL, MacKenzie CR. A new method of classifying prognostic comorbidity in longitudinal studies: development and validation. *Journal of chronic diseases*. 1987;40(5):373-383.

47. Weaver DJ, Malik AT, Jain N, Yu E, Kim J, Khan SN. The Modified 5-Item Frailty Index: A Concise and Useful Tool for Assessing the Impact of Frailty on Postoperative Morbidity Following Elective Posterior Lumbar Fusions. *World Neurosurgery*. 2019;124:e626-e632. doi:https://doi.org/10.1016/j.wneu.2018.12.168

48. Traven SA, Reeves RA, Sekar MG, Slone HS, Walton ZJ. New 5-Factor Modified Frailty Index Predicts Morbidity and Mortality in Primary Hip and Knee Arthroplasty. *Journal of Arthroplasty*. 2019;34(1):140-144. doi:10.1016/j.arth.2018.09.040

49. Robinson TN, Eiseman B, Wallace JI, et al. Redefining Geriatric Preoperative Assessment Using Frailty, Disability and Co-Morbidity. *Annals of Surgery*. 2009;250(3). https://journals.lww.com/annalsofsurgery/Fulltext/2009/09000/Redefining_Geriatric_Preoperative_Assessment_Using.13.aspx

50. Ening G, Osterheld F, Capper D, Schmieder K, Brenke C. Charlson comorbidity index: an additional prognostic parameter for preoperative glioblastoma patient stratification. *Journal of Cancer Research and Clinical Oncology*. 2015;141(6):1131-1137. doi:10.1007/s00432-014-1907-9

51. Hall WH, Ramachandran R, Narayan S, Jani AB, Vijayakumar S. An electronic application for rapidly calculating Charlson comorbidity score. *BMC Cancer*. 2004;4:1-8. doi:10.1186/1471-2407-4-94

52. Schag CC, Heinrich RL, Ganz PA. Karnofsky performance status revisited: reliability, validity, and guidelines. *Journal of Clinical Oncology*. 1984;2(3):187-193.

53. Banks JL, Marotta CA. Outcomes validity and reliability of the modified Rankin scale: implications for stroke clinical trials: a literature review and synthesis. *Stroke*. 2007;38(3):1091-1096.

54. Liu Y, Nickleach D, Zhang C, Switchenko J, Kowalski J. Carrying out streamlined routine data analyses with reports for observational studies: introduction to a series of generic SAS macros [version 2; peer review: 2 approved]. *F1000Research*. 2019;7(1955). doi:10.12688/f1000research.16866.2

55. Rupji M, Dwivedi B, Kowalski J. NOJAH: NOt Just Another Heatmap for genome-wide cluster analysis. *PLOS ONE*. 2019;14(3):1-14. doi:10.1371/journal.pone.0204542

56. Isensee F, Schell M, Pflueger I, et al. Automated brain extraction of multisequence MRI using artificial neural networks. *Hum Brain Mapp*. 2019;40(17):4952-4964. doi:10.1002/hbm.24750

57. Pérez-García F, Sparks R, Ourselin S. TorchIO: A Python library for efficient loading, preprocessing, augmentation and patch-based sampling of medical images in deep learning. *Computer Methods and Programs in Biomedicine*. 2021;208:106236. doi:https://doi.org/10.1016/j.cmpb.2021.106236

58. Miller KD, Ostrom QT, Kruchko C, et al. Brain and other central nervous system tumor statistics, 2021. *CA A Cancer J Clin*. 2021;71(5):381-406. doi:10.3322/caac.21693

59. Tabouret E, Chinot O, Metellus P, Tallet A, Viens P, Gonçalves A. Recent Trends in Epidemiology of Brain Metastases: An Overview. *ANTICANCER RESEARCH*. Published online 2012.

60. Molinaro AM, Hervey-Jumper S, Morshed RA, et al. Association of Maximal Extent of Resection of Contrast-Enhanced and Non–Contrast-Enhanced Tumor With Survival Within Molecular Subgroups of Patients With Newly Diagnosed Glioblastoma. *JAMA Oncology*. 2020;6(4):495-503. doi:10.1001/jamaoncol.2019.6143

61. Grabowski MM, Recinos PF, Nowacki AS, et al. Residual tumor volume versus extent of resection: predictors of survival after surgery for glioblastoma: Clinical article. *Journal of Neurosurgery JNS*. 2014;121(5):1115-1123. doi:10.3171/2014.7.JNS132449

62. Weller M, van den Bent M, Preusser M, et al. EANO guidelines on the diagnosis and treatment of diffuse gliomas of adulthood. *Nat Rev Clin Oncol*. 2021;18(3):170-186. doi:10.1038/s41571-020-00447-z

63. Khalafallah AM, Huq S, Jimenez AE, Brem H, Mukherjee D. The 5-factor modified frailty index: an effective predictor of mortality in brain tumor patients. *Journal of Neurosurgery*. Published online 2020:1-9. doi:10.3171/2020.5.jns20766

64. Lee SY, Song XY. Evaluation of the Bayesian and Maximum Likelihood Approaches in Analyzing Structural Equation Models with Small Sample Sizes. *Multivariate Behavioral Research*. 2004;39(4):653-686. doi:10.1207/s15327906mbr3904_4

65. Buchwald ZS, Tian S, Rossi M, et al. Genomic copy number variation correlates with survival outcomes in WHO grade IV glioma. *Scientific Reports*. 2020;10(1):1-10. doi:10.1038/s41598-020-63789-9

66. Hieronymus H, Murali R, Tin A, et al. Tumor copy number alteration burden is a pan-cancer prognostic factor associated with recurrence and death. Green MR, Settleman J, Abate-Shen C, Rubin MA, eds. *eLife*. 2018;7:e37294. doi:10.7554/eLife.37294

67. The Cancer Genome Atlas Research Network, Levine DA. Integrated genomic characterization of endometrial carcinoma. *Nature*. 2013;497(7447):67-73. doi:10.1038/nature12113

68. Mirchia K, Snuderl M, Galbraith K, Hatanpaa KJ, Walker JM, Richardson TE. Establishing a prognostic threshold for total copy number variation within adult IDH-mutant grade II/III astrocytomas. *Acta Neuropathologica Communications*. 2019;7(1):121. doi:10.1186/s40478-019-0778-3

69. Bumes E, Wirtz FP, Fellner C, et al. Non-Invasive Prediction of IDH Mutation in Patients with Glioma WHO II/III/IV Based on F-18-FET PET-Guided In Vivo 1H-Magnetic Resonance Spectroscopy and Machine Learning. *Cancers*. 2020;12(11):3406. doi:10.3390/cancers12113406

70. Jiang S, Zanazzi GJ, Hassanpour S. Predicting prognosis and IDH mutation status for patients with lower-grade gliomas using whole slide images. *Sci Rep*. 2021;11(1):16849. doi:10.1038/s41598-021-95948-x

71. Kandalgaonkar P, Sahu A, Saju AC, et al. Predicting IDH subtype of grade 4 astrocytoma and glioblastoma from tumor radiomic patterns extracted from multiparametric magnetic resonance images using a machine learning approach. *Front Oncol*. 2022;12:879376. doi:10.3389/fonc.2022.879376

72. Jakola AS, Pedersen LK, Skjulsvik AJ, Myrmel K, Sjåvik K, Solheim O. The impact of resection in IDH-mutant WHO grade 2 gliomas: a retrospective population-based parallel cohort study. *Journal of Neurosurgery*. 2022;137(5):1321-1328. doi:10.3171/2022.1.JNS212514

73. Wu AS, Witgert ME, Lang FF, et al. Neurocognitive function before and after surgery for insular gliomas: Clinical article. *Journal of Neurosurgery JNS*. 2011;115(6):1115-1125. doi:10.3171/2011.8.JNS11488

74. Satoer D, Vork J, Visch-Brink E, Smits M, Dirven C, Vincent A. Cognitive functioning early after surgery of gliomas in eloquent areas: Clinical article. *Journal of Neurosurgery JNS*. 2012;117(5):831-838. doi:10.3171/2012.7.JNS12263

Tables:

Table 1: Cohort characteristics, dichotomized by CCI ≥ 3 and mFI-5 ≥1.

		Charlson Comorbidity Index		5-Factor Modified Frailty Index	
Variables, n(%)	**Total Cohort**	**CCI = 0 - 2**, N = 118[1]	**CCI ≥ 3** , N = 18[1]	**mFI = 0**, N = 102[1]	**mFI-5 ≥ 1**, N = 34[1]
Age at Surgery, Years	38 (31, 47)	37 (30, 43)	63 (56, 73)	36 (30, 43)	48 (39, 62)
Male Sex	84 (62%)	74 (63%)	10 (56%)	62 (61%)	22 (65%)
Race					
White	111 (82%)	97 (82%)	14 (78%)	83 (81%)	28 (82%)
African-American	14 (10%)	14 (12%)	0 (0%)	10 (9.8%)	4 (12%)
Latino	5 (3.7%)	4 (3.4%)	1 (5.6%)	5 (4.9%)	0 (0%)
Asian	1 (0.7%)	1 (0.8%)	0 (0%)	1 (1.0%)	0 (0%)
Other	3 (2.2%)	2 (1.7%)	1 (5.6%)	3 (2.9%)	0 (0%)
Not Reported	2 (1.5%)	0 (0%)	2 (11%)	0 (0%)	2 (5.9%)
Body Mass Index (kg/m^2)	26.7 (23.7, 31.7)	26.3 (23.6, 30.3)	30.2 (24.4, 37.0)	26.3 (23.8, 29.8)	30.1 (23.4, 34.4)
Missing	10 (7%)	7 (6%)	3 (17%)	6 (6%)	4 (12%)
Preop Karnofsky Performance Status ≥ 70	124 (91%)	113 (96%)	11 (61%)	100 (98%)	24 (71%)
Preop Seizures	85 (62%)	73 (62%)	12 (67%)	63 (62%)	22 (65%)
Preop Neurological Deficit	45 (33%)	34 (29%)	11 (61%)	26 (25%)	19 (56%)
Tumor Location					
Frontal	85 (62%)	74 (63%)	11 (61%)	65 (64%)	20 (59%)
Parietal	13 (9.6%)	11 (9.3%)	2 (11%)	8 (7.8%)	5 (15%)
Temporal	29 (21%)	26 (22%)	3 (17%)	24 (24%)	5 (15%)
Occipital	6 (4.4%)	5 (4.2%)	1 (5.6%)	4 (3.9%)	2 (5.9%)
Insula	2 (1.5%)	1 (0.8%)	1 (5.6%)	1 (1.0%)	1 (2.9%)
Cerebellum	1 (0.7%)	1 (0.8%)	0 (0%)	0 (0%)	1 (2.9%)
Left-Sided Tumor	75 (55%)	66 (56%)	9 (50%)	57 (56%)	18 (53%)
Tumor Primarily Centered Outside Deep Structures	99 (73%)	88 (75%)	11 (65%)	75 (74%)	24 (73%)
Missing	1	0	1	0	1
Tumor Centered in Eloquent Location	61 (46%)	52 (44%)	9 (53%)	44 (43%)	17 (53%)
Missing	2	1	1	0	2

Type of Surgery					
Stereotactic Biopsy	47 (35%)	37 (31%)	10 (56%)	36 (35%)	11 (32%)
Open Biopsy	2 (1.5%)	1 (0.8%)	1 (5.6%)	1 (1.0%)	1 (2.9%)
Craniotomy for Resection	87 (64%)	80 (68%)	7 (39%)	65 (64%)	22 (65%)
Astrocytic Lineage (vs. Oligodendroglioma)	87 (64%)	80 (68%)	7 (39%)	68 (67%)	19 (56%)
Total # Copy Number Variations	9 (5, 18)	10 (5, 17)	8 (5, 31)	10 (5, 17)	8 (5, 26)
Missing	43	38	5	31	12
Immediate Postoperative Neurological Deficit					
None	112 (82%)	100 (85%)	12 (67%)	86 (84%)	26 (76%)
Motor	12 (8.8%)	6 (5.1%)	6 (33%)	5 (4.9%)	7 (21%)
Sensory	2 (1.5%)	2 (1.7%)	0 (0%)	2 (2.0%)	0 (0%)
Language	6 (4.4%)	6 (5.1%)	0 (0%)	6 (5.9%)	0 (0%)
Visual	2 (1.5%)	2 (1.7%)	0 (0%)	2 (2.0%)	0 (0%)
Other	2 (1.5%)	2 (1.7%)	0 (0%)	1 (1.0%)	1 (2.9%)
Postop Karnofsky Performance Status $\geq$ 70	124 (91%)	114 (97%)	10 (56%)	100 (98%)	24 (71%)
Adjuvant Temozolomide Use	106 (84%)	96 (85%)	10 (77%)	82 (84%)	24 (86%)
Missing	10	5	5	4	6
Adjuvant Radiation Use	100 (74%)	90 (76%)	10 (56%)	78 (76%)	22 (65%)
Median Time to Death	36 (18, 77)	55 (25, 94)	13 (6, 24)	55 (25, 90)	14 (6, 32)
Missing	113	99	14	85	28
30-Day Readmission	8 (5.9%)	7 (5.9%)	1 (5.6%)	5 (4.9%)	3 (8.8%)

[1]Median (IQR); n (%)
Abbreviations: CCI: Charlson Comorbidity Index, mFI-5: 5-factor modified frailty index, #: number

Table 2. Results from multivariable adjusted models for effect of frailty upon 30-day readmission.

		Odds of 30-day readmission, n=136		
Frailty Metric	**N (%)**	**Crude OR (95%CI)**	**aOR (95% CI)**	**P-value**
CCI 0 – 2	118 (87)	REF	REF	
CCI ≥ 3	18 (13)	0.93 (0.04 – 5.72)	0.22 (0.01 – 3.24)[a]	0.30
mFI-5 = 0	102 (75)	REF	REF	
mFI-5 ≥ 1	34 (25)	1.88 (0.37 – 8.10)	1.56 (0.24 – 8.96)[b]	0.62

Abbreviations: OR: odds ratio; aOR: adjusted odds ratio; 95% CI: 95% confidence interval; REF: reference.

[a]Model adjusted for tumor location, BMI, type of surgery, and age, model n=125

[b]Model adjusted for tumor location, BMI, type of surgery, and age, model n=125

Table 3. Results from adjusted models for effect of frailty upon overall survival.

			Hazard ratio for rate of overall survival, n=136		
Frailty Metric	**Death N (%)**	**Median months to death (IQR)**	**Crude HR (95%CI)**	**aHR (95% CI)**	**P-value**
CCI 0 - 2	19 (83)	55.3 (22.0, 99.1)	REF	REF	
CCI ≥ 3	4 (17)	11.1 (1.1, 58.0)	3.33 (1.12 – 9.97)	0.59 (0.05 – 6.37)[a]	0.7
mFI-5 = 0	17 (74)	63.1 (31.6, 99.8)	REF	REF	
mFI-5 ≥ 1	6 (16)	26.3 (2.5, 55.3)	2.14 (0.83 – 5.47)	1.15 (0.29 – 4.52)[b]	0.8

Abbreviations: HR: hazard ratio; aHR: adjusted hazard ratio; 95% CI: 95% confidence interval; REF: reference.

[a]Model adjusted for age, tumor location, BMI, and type of surgery, history of prior surgery; model n=125

[b]Model adjusted for age, tumor location, BMI, and type of surgery, history of prior surgery; model n=125

Table 4: Adjusted hazard ratio of death in patients with de novo tumors/new diagnosis (n = 99).

Variable	**HR**[1]	**95% CI**[1]	**p-value**
mFI = 0	REF	REF	REF
mFI >=1	**6.79**	**1.00, 45.9**	**0.049**
Age at Surgery	1.01	0.96, 1.07	0.6
Convexity Location	0.50	0.13, 1.99	0.3
BMI	0.81	0.69, 0.94	0.006
Open craniotomy for resection	3.22	0.84, 12.4	0.088
[1]HR = Hazard Ratio, CI = Confidence Interval			

Table 5: Descriptive statistics of copy number variation [CNV] (mutational burden of tumor) per glioma, and distribution of CNV for overall survival (OS) and progression free survival (PFS).

Variable	Level	N (%) = 93
CNV total (categorical)	<= 8.5 (median)	44 (50.0)
	> 8.5 (median)	44 (50.0)
	Missing	5
CNV Cutpoint for OS	<= 10.5 (Optimal cutoff)	50 (56.8)
	> 10.5 (Optimal cutoff)	38 (43.2)
	Missing	5
CNV Cutpoint for PFS	<= 7.5 (Optimal cutoff)	40 (45.5)
	> 7.5 (Optimal cutoff)	48 (54.5)
	Missing	5
CNV	Mean	12.80
	Median	8.50
	Minimum	1.00
	Maximum	58.00
	Std Dev	11.36
	Missing	5.00

Table 6: Training imaging-only model evaluation (n = 87).

Measure	Value	Derivations
Sensitivity	0.9032	TPR = TP / (TP + FN)
Specificity	0.9592	SPC = TN / (FP + TN)
Precision	0.9333	PPV = TP / (TP + FP)
Negative Predictive Value	0.9400	NPV = TN / (TN + FN)
False Positive Rate	0.0408	FPR = FP / (FP + TN)
False Discovery Rate	0.0667	FDR = FP / (FP + TP)
False Negative Rate	0.0968	FNR = FN / (FN + TP)
Accuracy	0.9375	ACC = (TP + TN) / (P + N)
F1 Score	0.9180	F1 = 2TP / (2TP + FP + FN)
Matthews Correlation Coefficient	0.8679	TP*TN - FP*FN / sqrt((TP+FP)*(TP+FN)*(TN+FP)*(TN+FN))

Table 7: Validation imaging-only model evaluation (n = 16)

Measure	Value	Derivations
Sensitivity	0.8000	TPR = TP / (TP + FN)
Specificity	0.8182	SPC = TN / (FP + TN)
Precision	0.6667	PPV = TP / (TP + FP)
Negative Predictive Value	0.9000	NPV = TN / (TN + FN)
False Positive Rate	0.1818	FPR = FP / (FP + TN)
False Discovery Rate	0.3333	FDR = FP / (FP + TP)
False Negative Rate	0.2000	FNR = FN / (FN + TP)
Accuracy	0.8125	ACC = (TP + TN) / (P + N)
F1 Score	0.7273	F1 = 2TP / (2TP + FP + FN)
Matthews Correlation Coefficient	0.5919	TP*TN - FP*FN / sqrt((TP+FP)*(TP+FN)*(TN+FP)*(TN+FN))

Figures

Figure 1: Cohort flow diagram

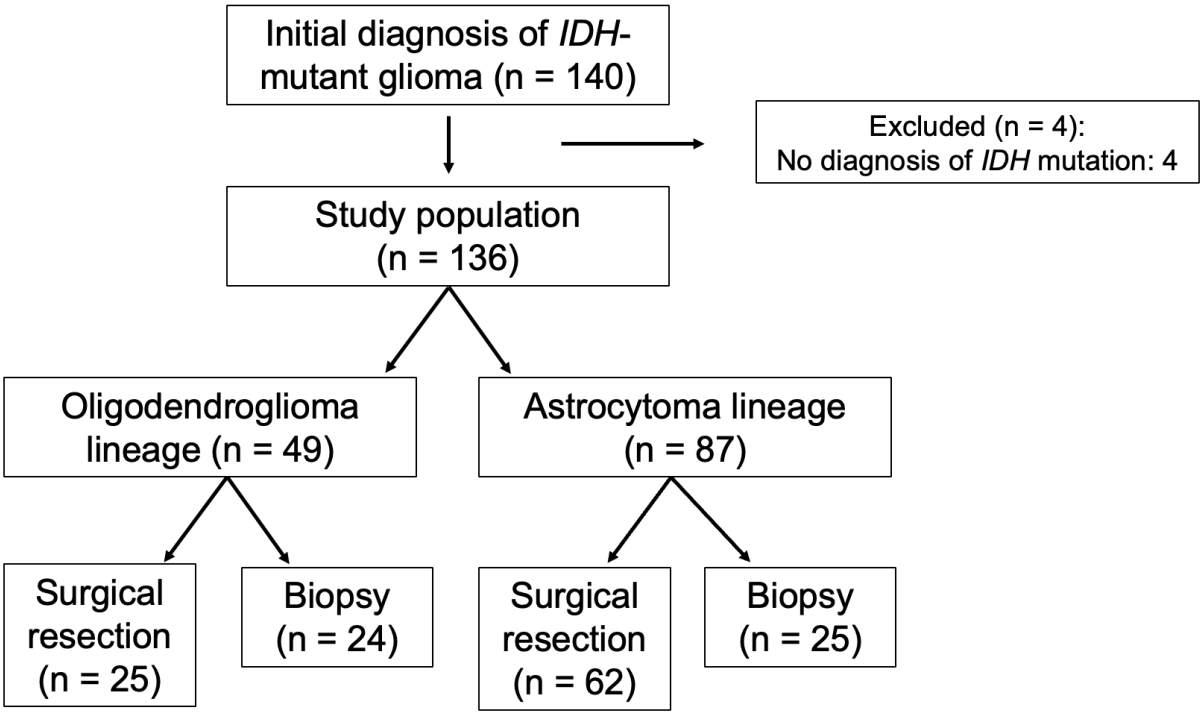

Figure 2: Glioma patient care flow diagram

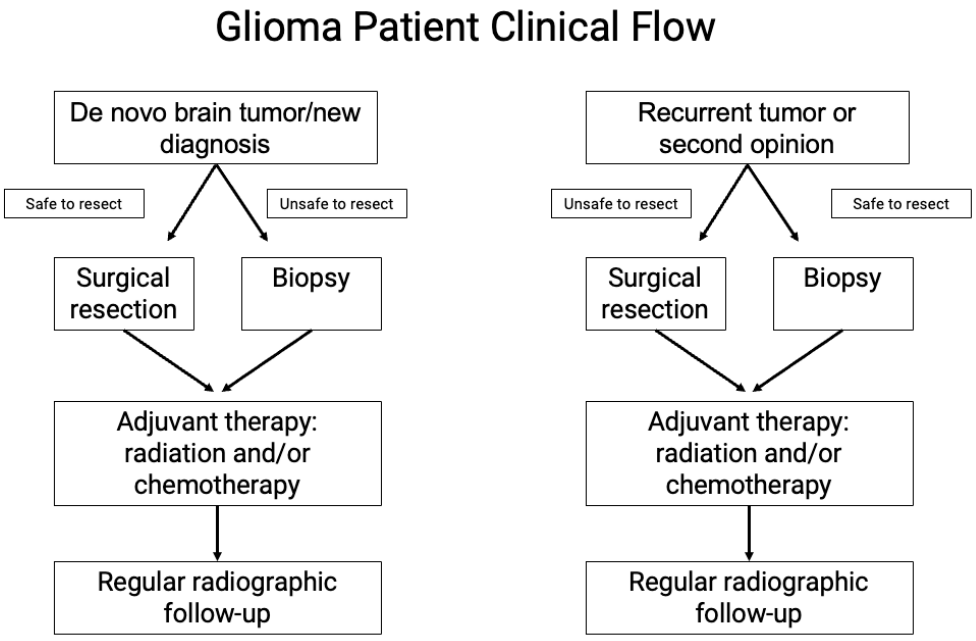

Figure 3: Directed acyclic graphs for exposure, outcome relationships. A. Frailty and 30 day hospital readmission, B. Frailty and overall survival.

A.

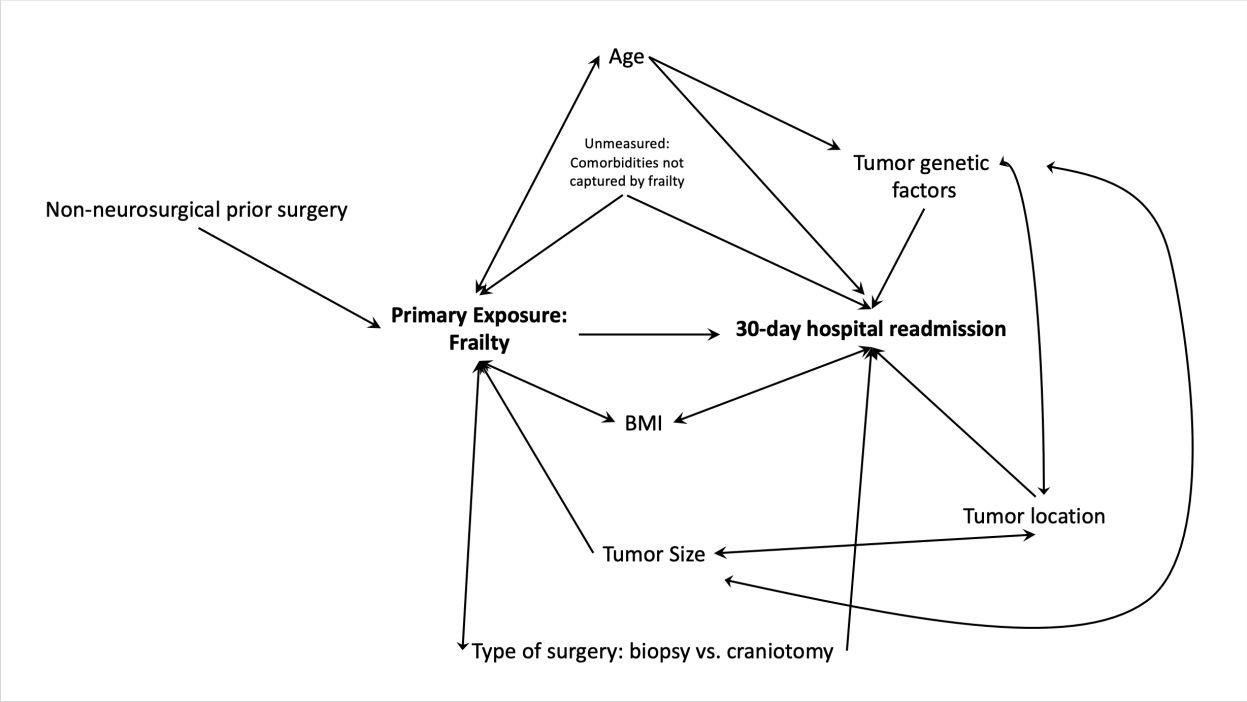

B.

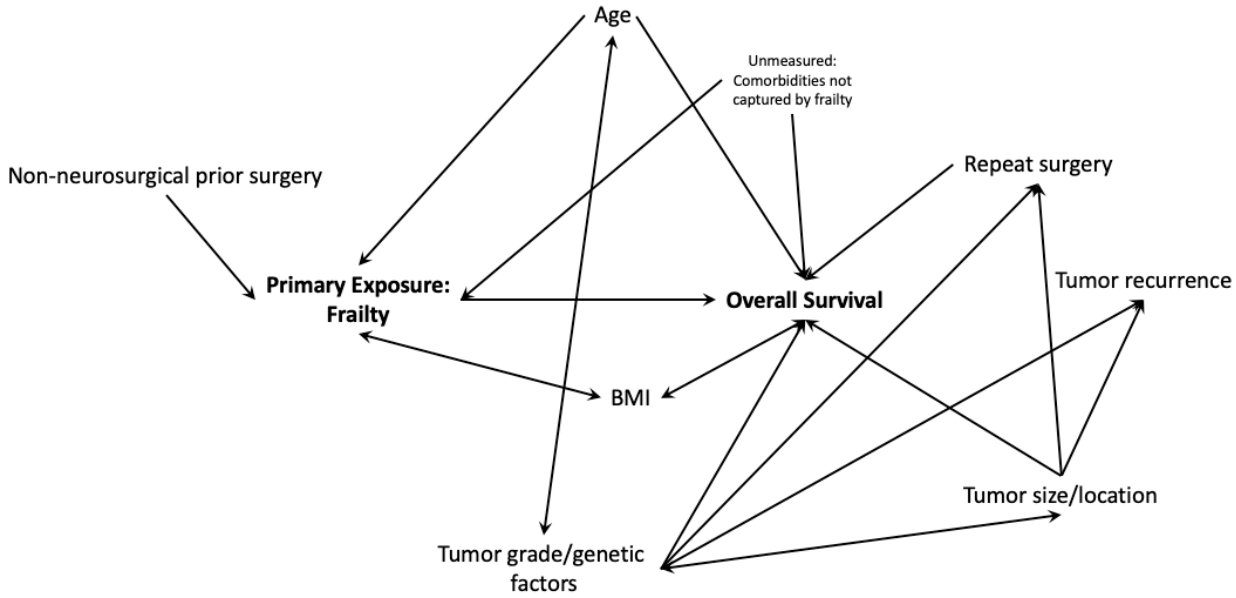

Figure 4: Kaplan-Meier survival curves for overall cohort, CCI ≥ 3 vs. CCI 0 – 2, and mFI-5 ≥ 1 vs. mFI-5 = 0.

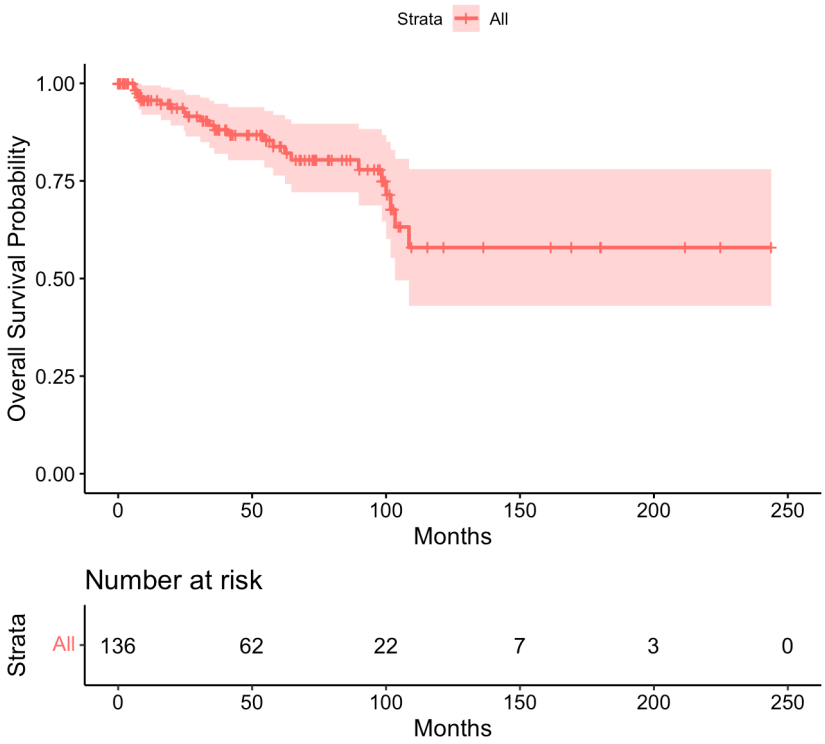

Figure 5: Kaplan-Meier survival curves for CCI ≥ 3 vs. CCI 0 – 2, and mFI-5 ≥ 1 vs. mFI-5 = 0.

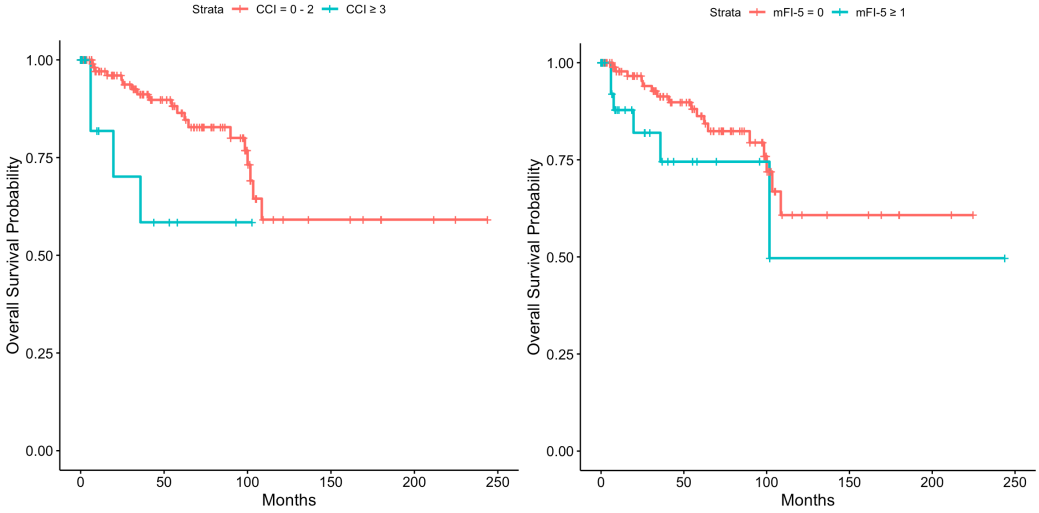

Figure 6: Kaplan-Meier survival curves for surgery vs. biopsy, and astrocytoma vs. oligodendroglioma.

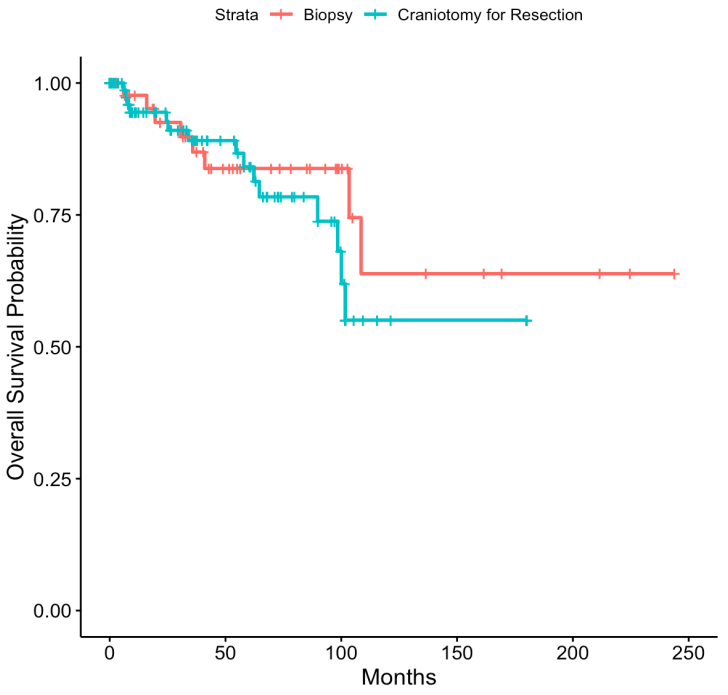

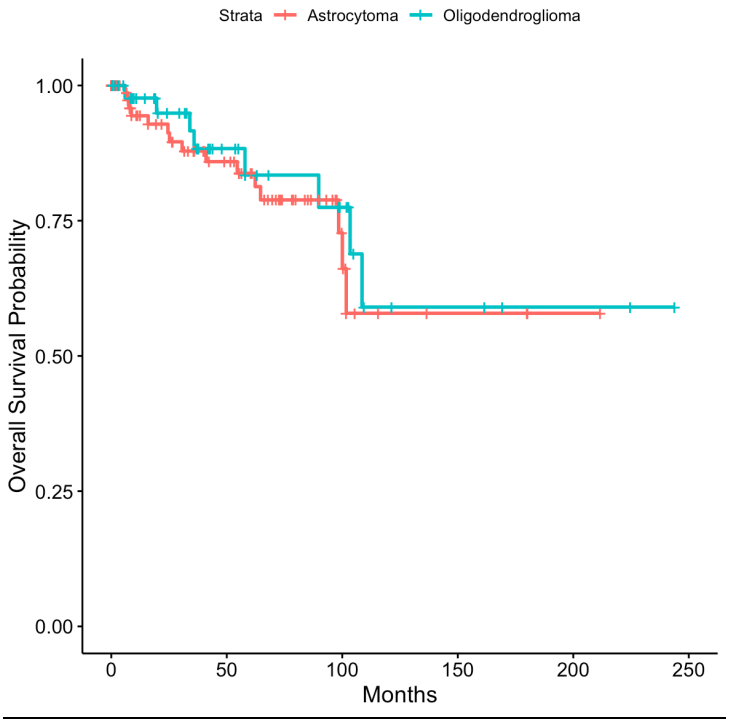

Genetic Analysis Figures:

Figure 7A Progression Free Survival (PFS) Kaplan Meier (KM) Curves – Copy Number Variation (CNV) median

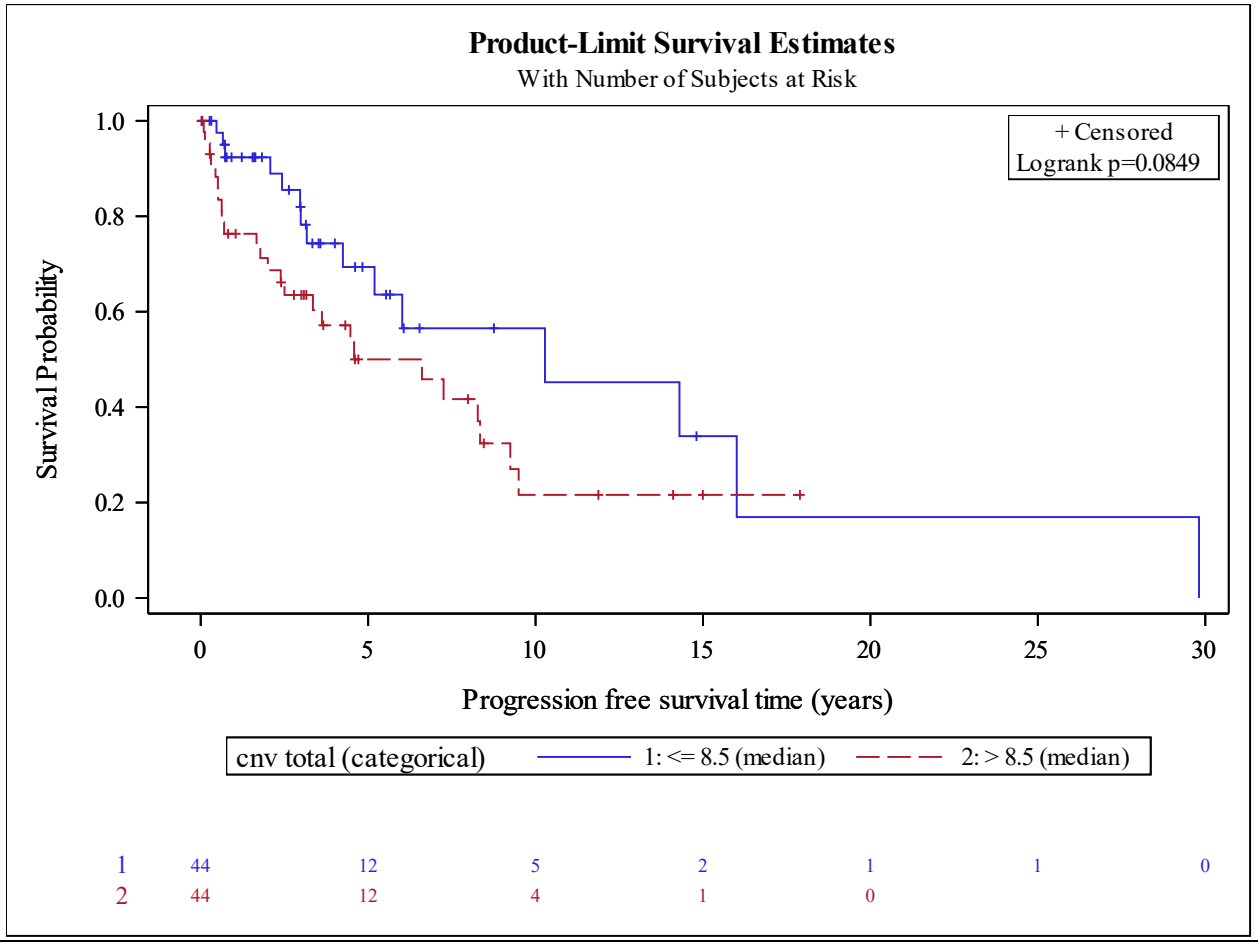

CNV Total (categorical)	No. of Subject	Event	Censored	Median Survival (95% CI)	1 Yr Survival	3 Yr Survival	5 Yr Survival	10 Yr Survival
<= 8.5 (median)	44	15 (34%)	29 (66%)	10.3 (4.2, 16)	92.4% (78.1%, 97.5%)	78.2% (59.2%, 89.1%)	69.4% (48.3%, 83.2%)	56.5% (32.8%, 74.7%)
> 8.5 (median)	44	25 (57%)	19 (43%)	6.6 (2.4, 8.3)	76.3% (60.5%, 86.5%)	63.5% (46.8%, 76.2%)	50.0% (32.7%, 65.1%)	21.6% (7.8%, 39.9%)

Figure 1B PFS KM Curves - CNV quartile

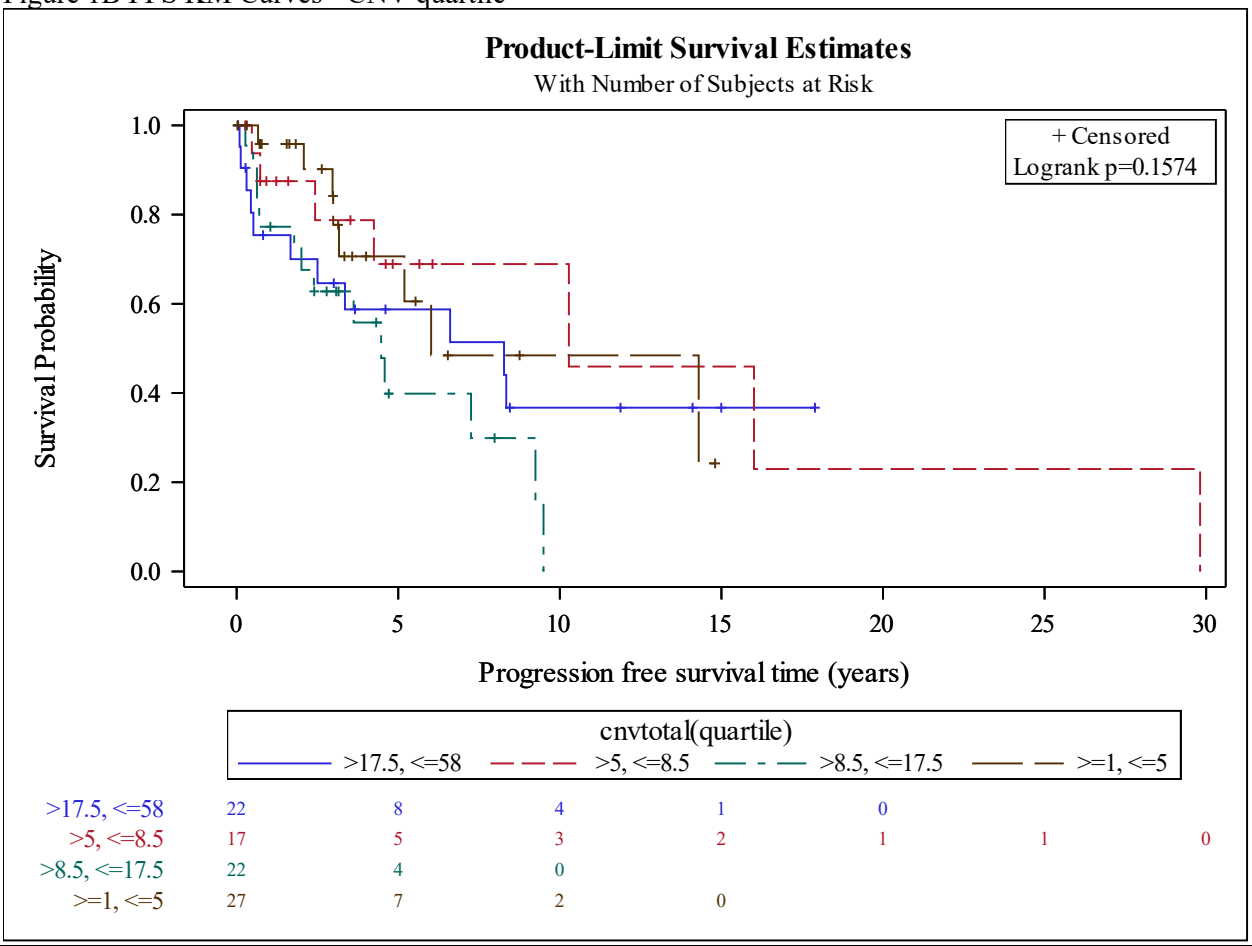

CNV Total (quartile)	No. of Subject	Event	Censored	Median Survival (95% CI)	1 Yr Survival	3 Yr Survival	5 Yr Survival	10 Yr Survival
>17.5, <=58	22	11 (50%)	11 (50%)	8.3 (1.7, NA)	75.4% (50.6%, 89.0%)	64.6% (39.6%, 81.4%)	58.8% (33.9%, 77.0%)	36.7% (14.5%, 59.4%)
>5, <=8.5	17	7 (41%)	10 (59%)	10.3 (2.4, 29.8)	87.5% (58.6%, 96.7%)	78.8% (46.6%, 92.8%)	68.9% (35.4%, 87.5%)	68.9% (35.4%, 87.5%)
>8.5, <=17.5	22	14 (64%)	8 (36%)	4.5 (1.8, 9.2)	77.3% (53.7%, 89.8%)	62.8% (39.1%, 79.4%)	39.9% (16.6%, 62.5%)	0.0% (NA, NA)
>=1, <=5	27	8 (30%)	19 (70%)	6 (3.2, NA)	95.8% (73.9%, 99.4%)	77.7% (50.3%, 91.2%)	70.6% (42.4%, 86.9%)	48.4% (18.2%, 73.4%)

Figure 1C PFS KM Curves - CNV Optimal cut point

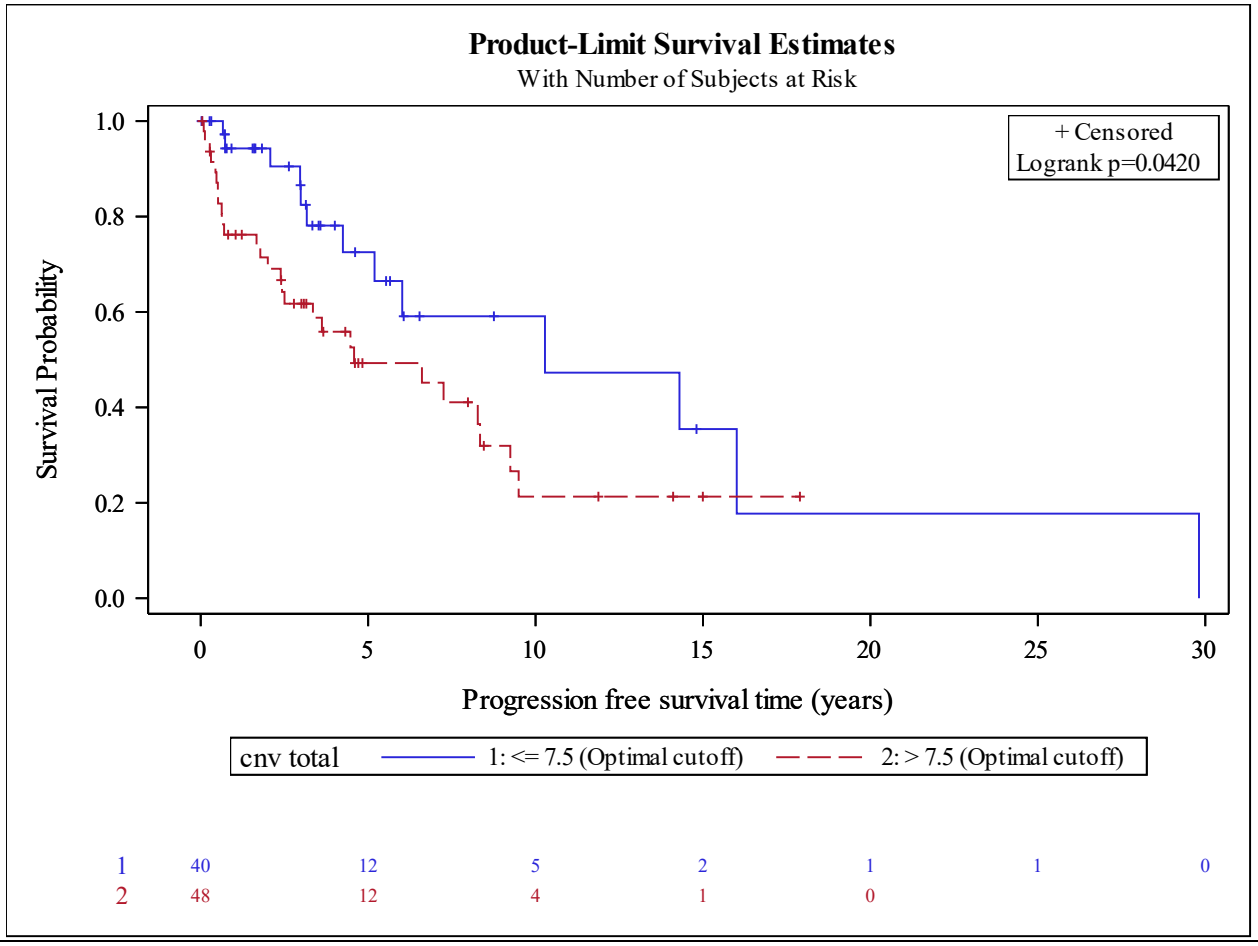

CNV Total	No. of Subject	Event	Censored	Median Survival (95% CI)	1 Yr Survival	3 Yr Survival	5 Yr Survival	10 Yr Survival
<= 7.5 (Optimal cutoff)	40	13 (33%)	27 (68%)	10.3 (4.2, 29.8)	94.3% (79.0%, 98.5%)	82.4% (62.4%, 92.4%)	72.5% (49.8%, 86.3%)	59.1% (33.8%, 77.5%)
> 7.5 (Optimal cutoff)	48	27 (56%)	21 (44%)	4.6 (2.4, 8.3)	76.2% (61.1%, 86.1%)	61.7% (45.7%, 74.3%)	49.3% (32.8%, 63.8%)	21.3% (7.7%, 39.3%)

Figure 8A Overall Survival (OS) KM Curves - CNV median

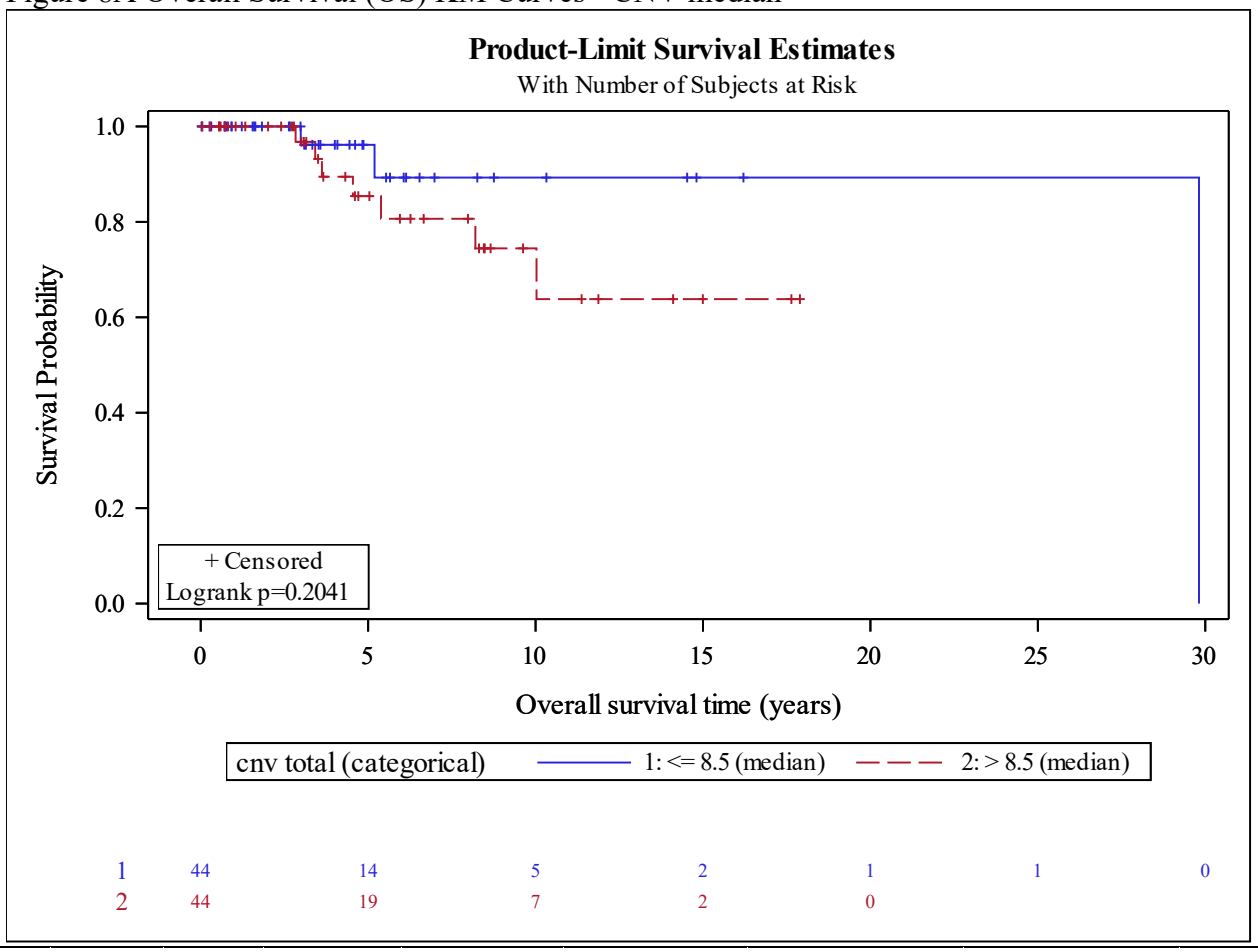

CNV total (categorical)	No. of Subject	Event	Censored	Median Survival (95% CI)	1 Yr Survival	3 Yr Survival	5 Yr Survival	10 Yr Survival
<= 8.5 (median)	44	3 (7%)	41 (93%)	29.8 (NA, NA)	100.0% (NA, NA)	96.2% (75.7%, 99.4%)	96.2% (75.7%, 99.4%)	89.3% (61.7%, 97.4%)
> 8.5 (median)	44	7 (16%)	37 (84%)	NA (10, NA)	100.0% (NA, NA)	96.8% (79.2%, 99.5%)	85.4% (65.4%, 94.3%)	74.4% (50.5%, 88.0%)

Figure 8B OS KM Curves - CNV quartile

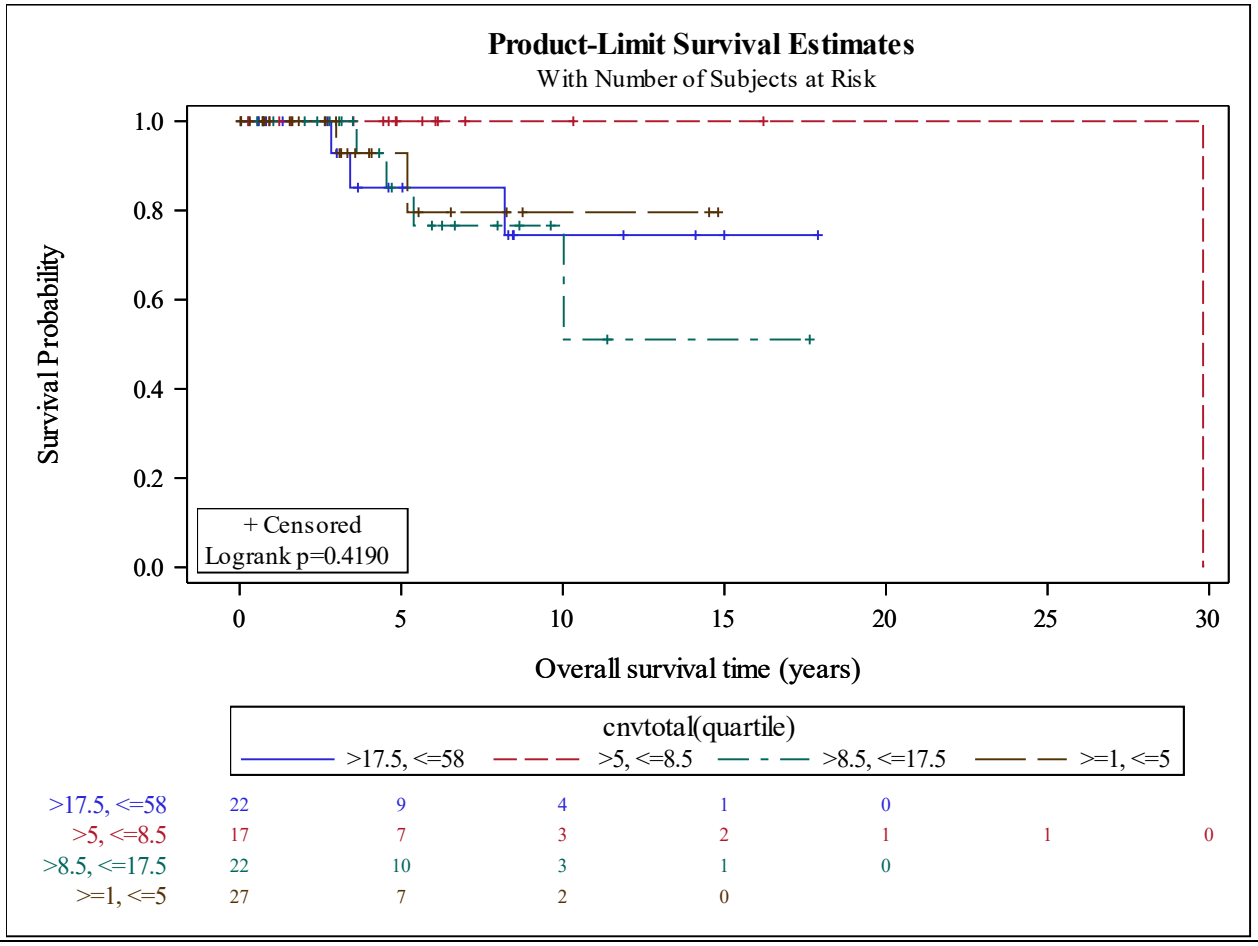

CNV Total (quartile)	No. of Subject	Event	Censored	Median Survival (95% CI)	1 Yr Survival	3 Yr Survival	5 Yr Survival	10 Yr Survival
>17.5, <=58	22	3 (14%)	19 (86%)	NA (8.2, NA)	100.0% (NA, NA)	92.9% (59.1%, 99.0%)	85.1% (52.3%, 96.1%)	74.5% (38.7%, 91.3%)
>5, <=8.5	17	1 (6%)	16 (94%)	29.8 (NA, NA)	100.0% (NA, NA)	100.0% (NA, NA)	100.0% (NA, NA)	100.0% (NA, NA)
>8.5, <=17.5	22	4 (18%)	18 (82%)	NA (5.4, NA)	100.0% (NA, NA)	100.0% (NA, NA)	85.1% (52.3%, 96.1%)	76.6% (43.3%, 91.9%)
>=1, <=5	27	2 (7%)	25 (93%)	NA (5.2, NA)	100.0% (NA, NA)	92.9% (59.1%, 99.0%)	92.9% (59.1%, 99.0%)	79.6% (37.1%, 94.9%)

Figure 8C OS KM Curves - CNV Optimal cut point

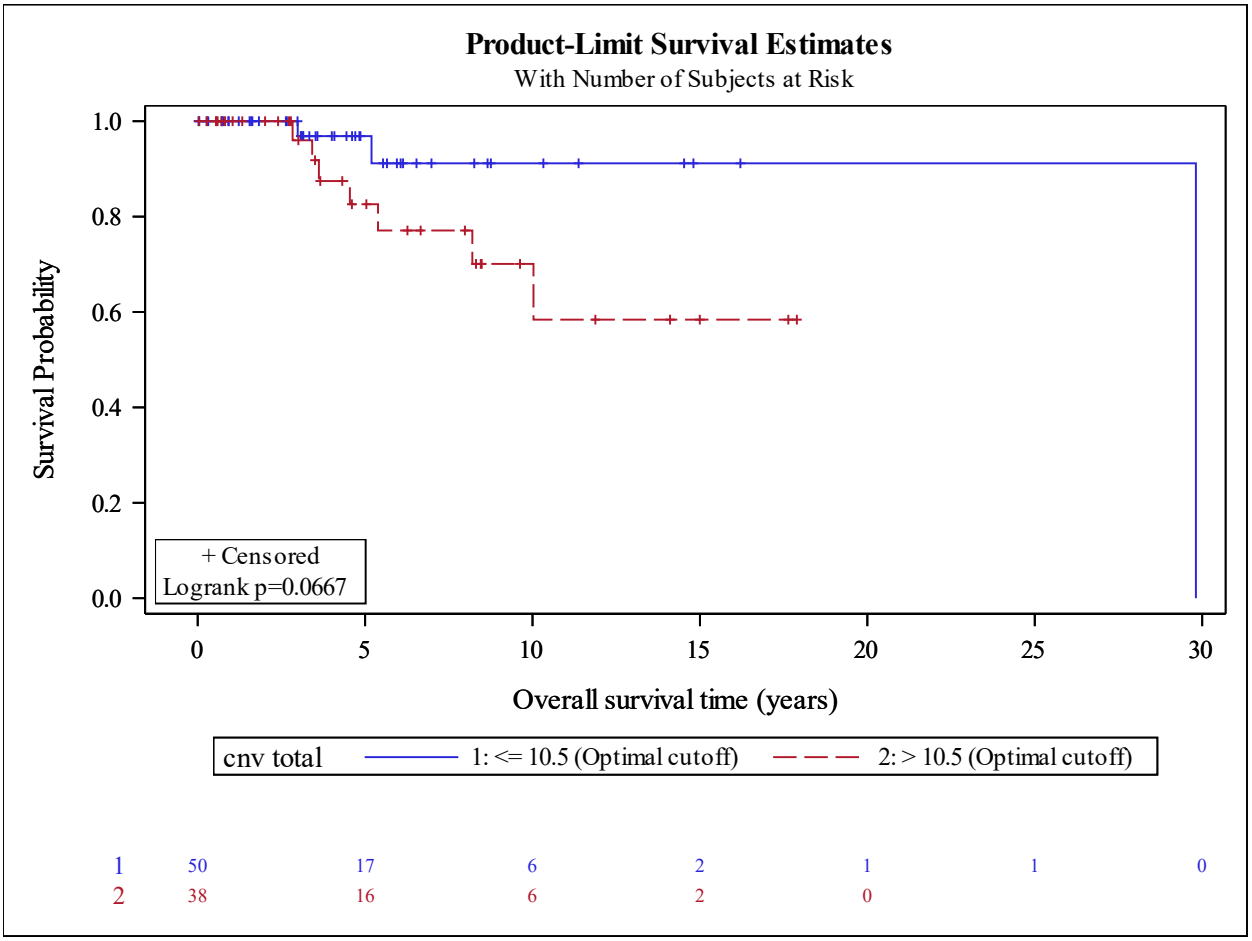

CNV Total	No. of Subject	Event	Censored	Median Survival (95% CI)	1 Yr Survival	3 Yr Survival	5 Yr Survival	10 Yr Survival
<= 10.5 (Optimal cutoff)	50	3 (6%)	47 (94%)	29.8 (NA, NA)	100.0% (NA, NA)	96.9% (79.8%, 99.6%)	96.9% (79.8%, 99.6%)	91.2% (67.4%, 97.9%)
> 10.5 (Optimal cutoff)	38	7 (18%)	31 (82%)	NA (8.2, NA)	100.0% (NA, NA)	96.0% (74.8%, 99.4%)	82.6% (59.8%, 93.1%)	70.1% (43.9%, 85.8%)

Figure 9A Spearman correlation plot CNV Total percentage with OS

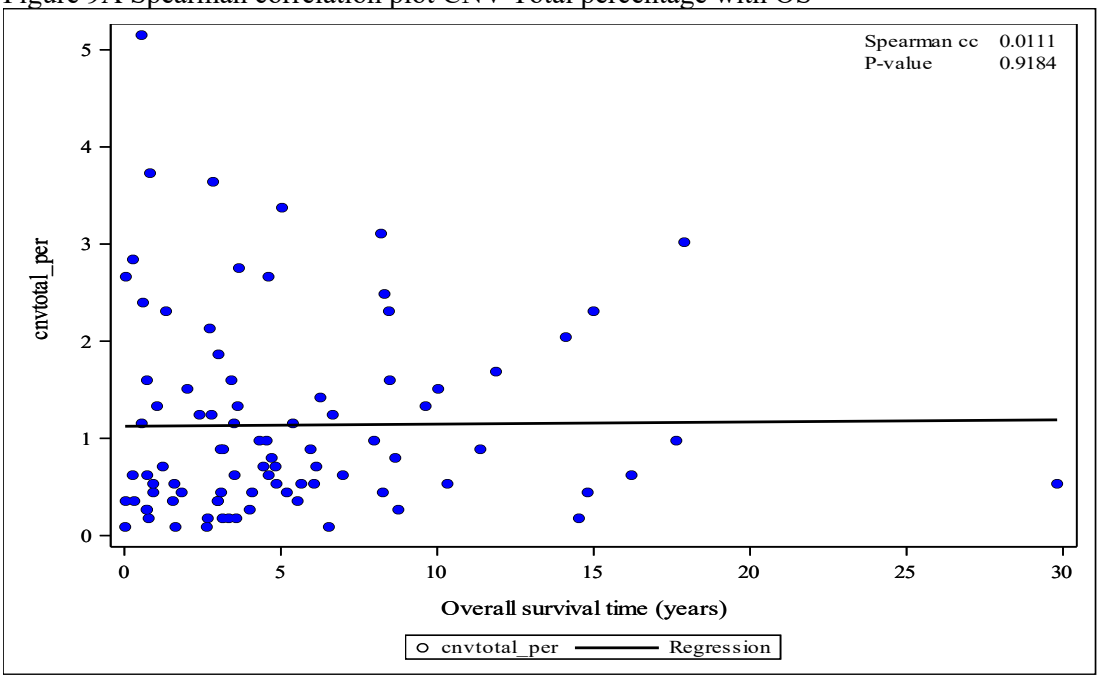

Figure 9B Spearman correlation plot CNV Total percentage with PFS

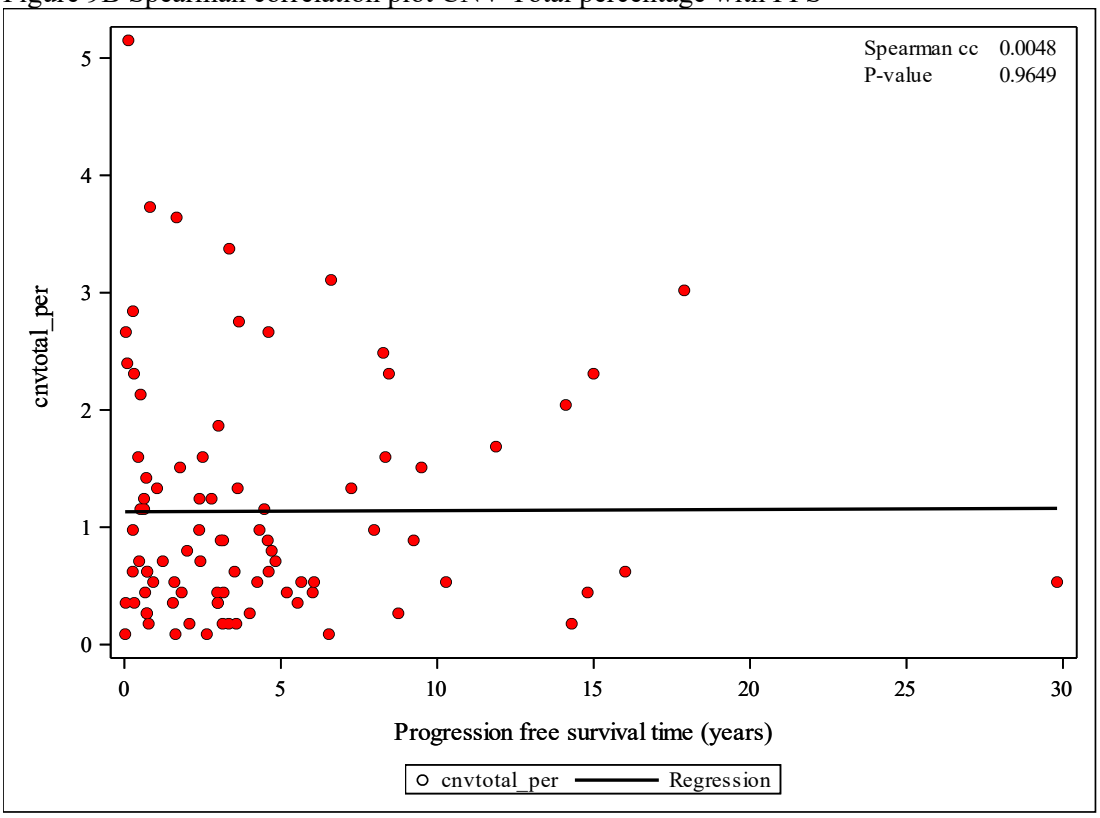

Figure 10A: Heatmap analysis; chromosome/gene amplification or deletion vs. none.

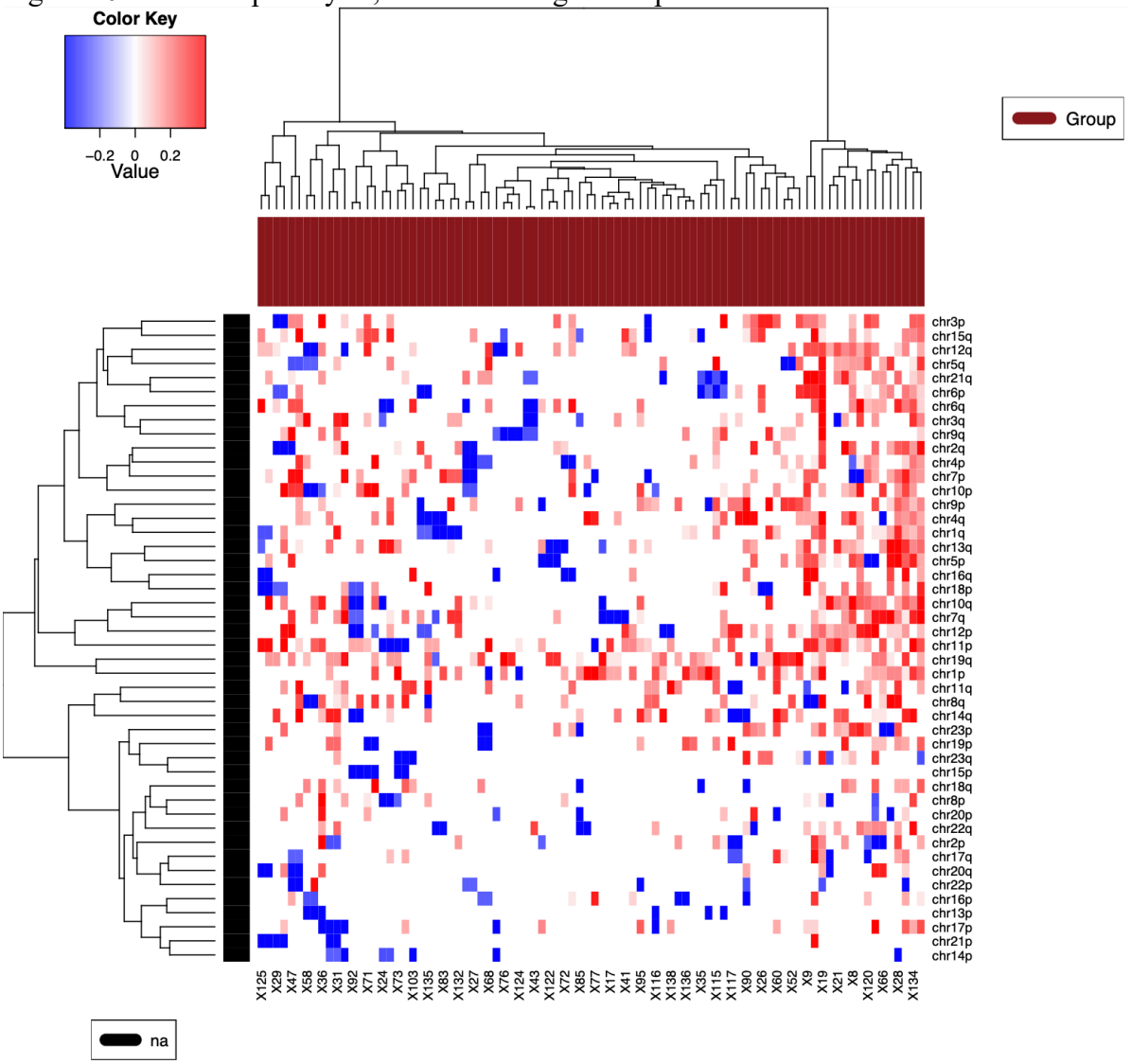

Figure 10B PFS KM Curves – Heat Map clusters – Gene Amplification or Deletion vs None

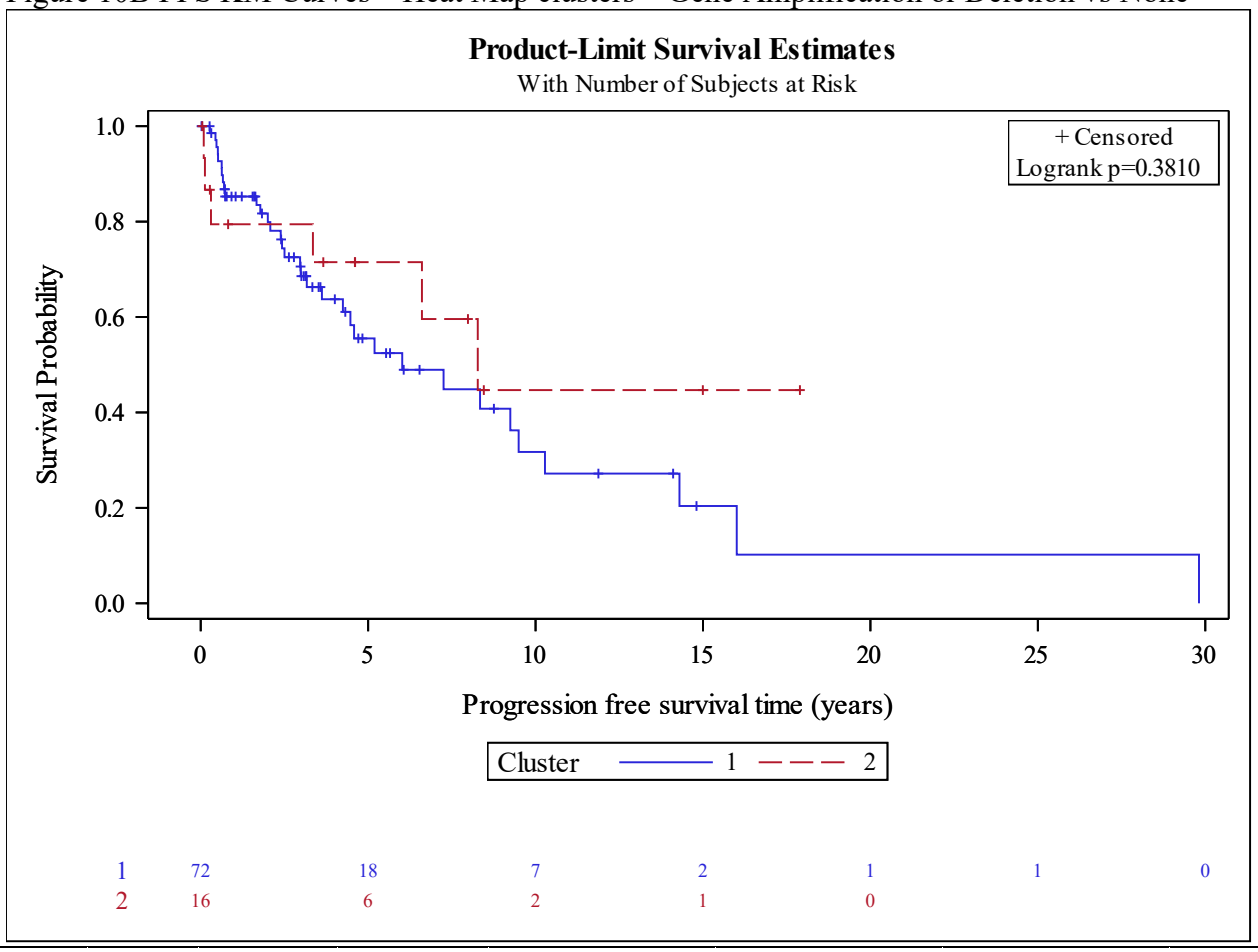

Cluster	No. of Subject	Event	Censored	Median Survival (95% CI)	1 Yr Survival	3 Yr Survival	5 Yr Survival	10 Yr Survival
1	72	34 (47%)	38 (53%)	6 (3.6, 9.5)	85.3% (74.3%, 91.8%)	68.6% (55.0%, 78.8%)	55.5% (40.3%, 68.3%)	31.7% (16.2%, 48.5%)
2	16	6 (38%)	10 (63%)	8.3 (0.3, NA)	79.4% (48.8%, 92.9%)	79.4% (48.8%, 92.9%)	71.5% (40.4%, 88.3%)	44.7% (13.0%, 72.7%)

Figure 10C OS KM Curves – Heat Map clusters – Gene Amplification or Deletion vs None

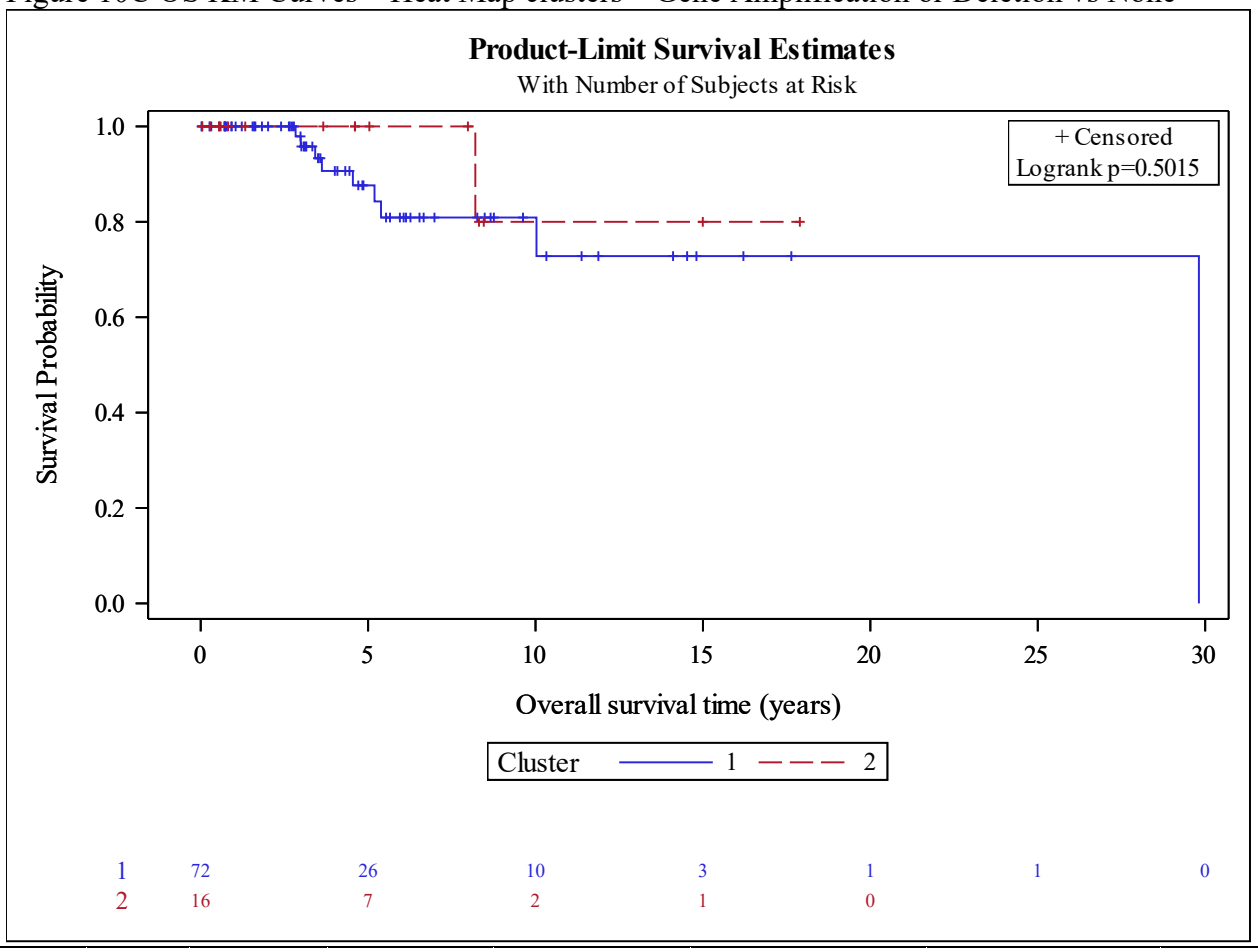

Cluster	No. of Subject	Event	Censored	Median Survival (95% CI)	1 Yr Survival	3 Yr Survival	5 Yr Survival	10 Yr Survival
1	72	9 (13%)	63 (88%)	29.8 (10, 29.8)	100.0% (NA, NA)	95.8% (84.2%, 98.9%)	87.6% (72.5%, 94.7%)	80.9% (63.5%, 90.6%)
2	16	1 (6%)	15 (94%)	NA (8.2, NA)	100.0% (NA, NA)	100.0% (NA, NA)	100.0% (NA, NA)	80.0% (20.4%, 96.9%)

Figure 11A: Heatmap analysis; chromosome/gene amplification vs deletion or loss of heterozygosity vs none.

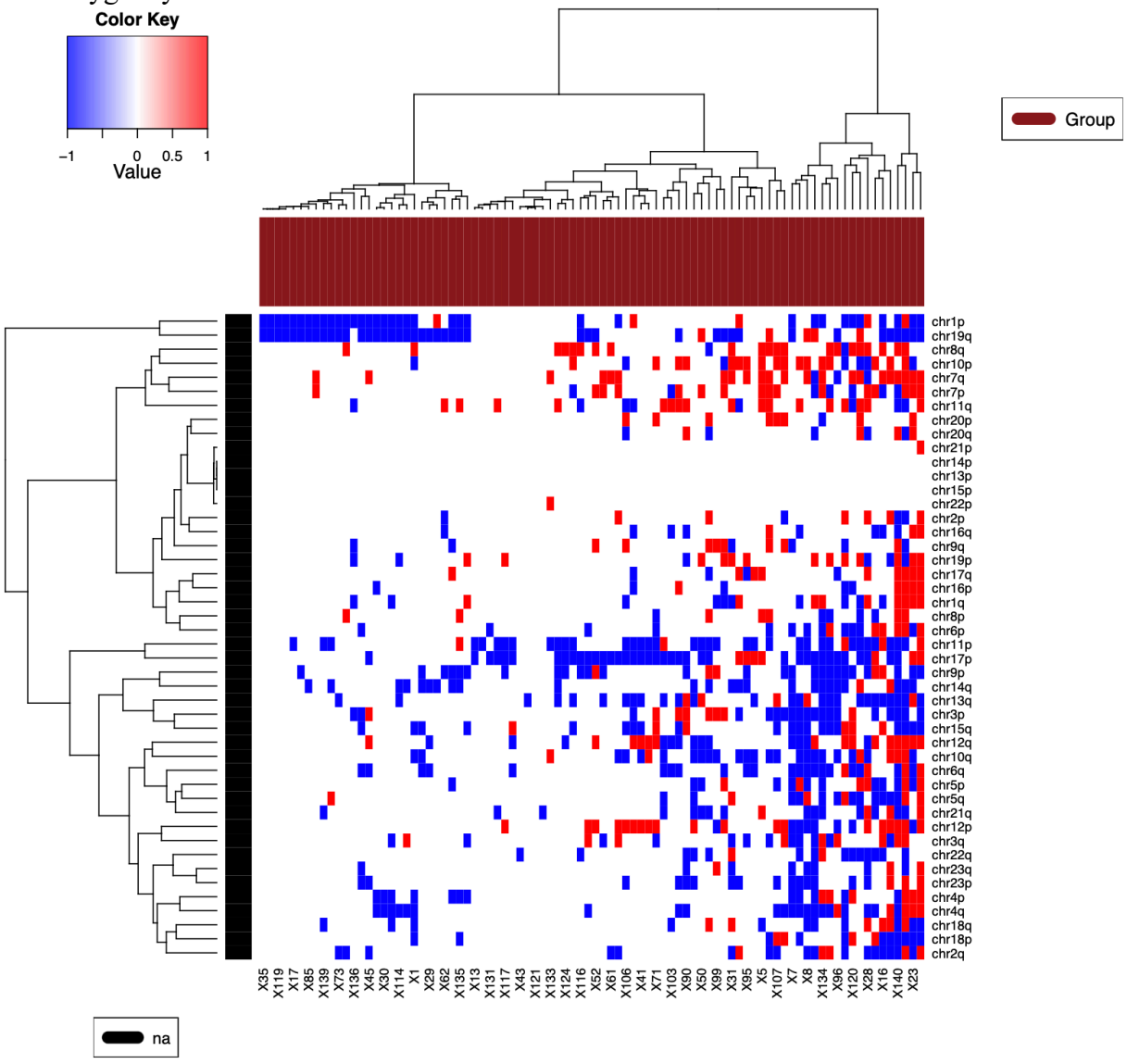

Figure 11B PFS KM Curves – Heat Map clusters – Gene Amplification vs Deletion or Loss of Heterozygosity vs None

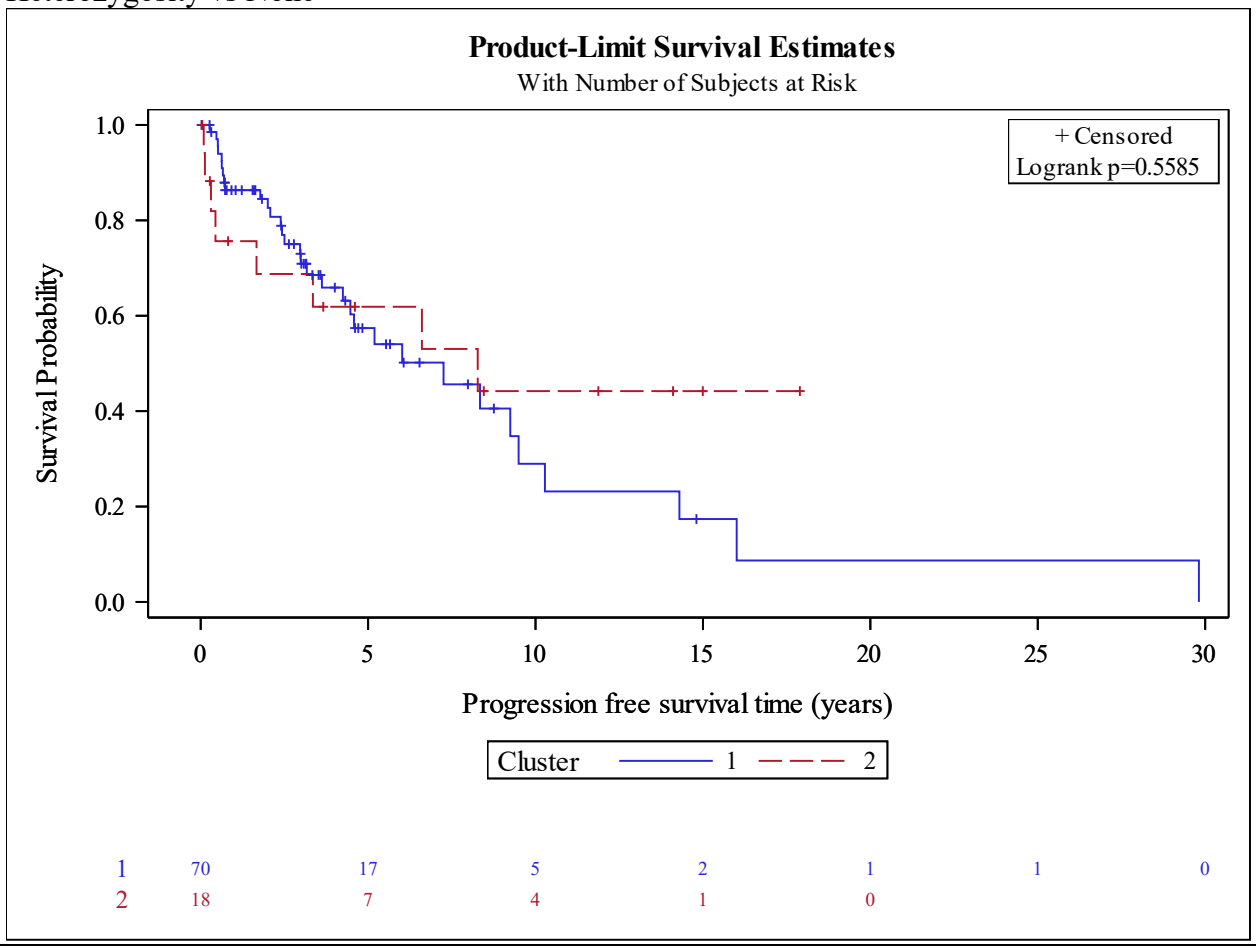

Cluster	No. of Subject	Event	Censored	Median Survival (95% CI)	1 Yr Survival	3 Yr Survival	5 Yr Survival	10 Yr Survival
1	70	32 (46%)	38 (54%)	7.3 (4.2, 9.5)	86.3% (75.4%, 92.6%)	70.9% (57.1%, 81.0%)	57.4% (41.8%, 70.2%)	29.0% (12.6%, 47.7%)
2	18	8 (44%)	10 (56%)	8.3 (0.4, NA)	75.6% (47.3%, 90.1%)	68.8% (40.2%, 85.7%)	61.9% (33.8%, 80.9%)	44.2% (17.8%, 67.9%)

Figure 11C OS KM Curves – Heat Map clusters - Amp vs deletion or LOH vs none

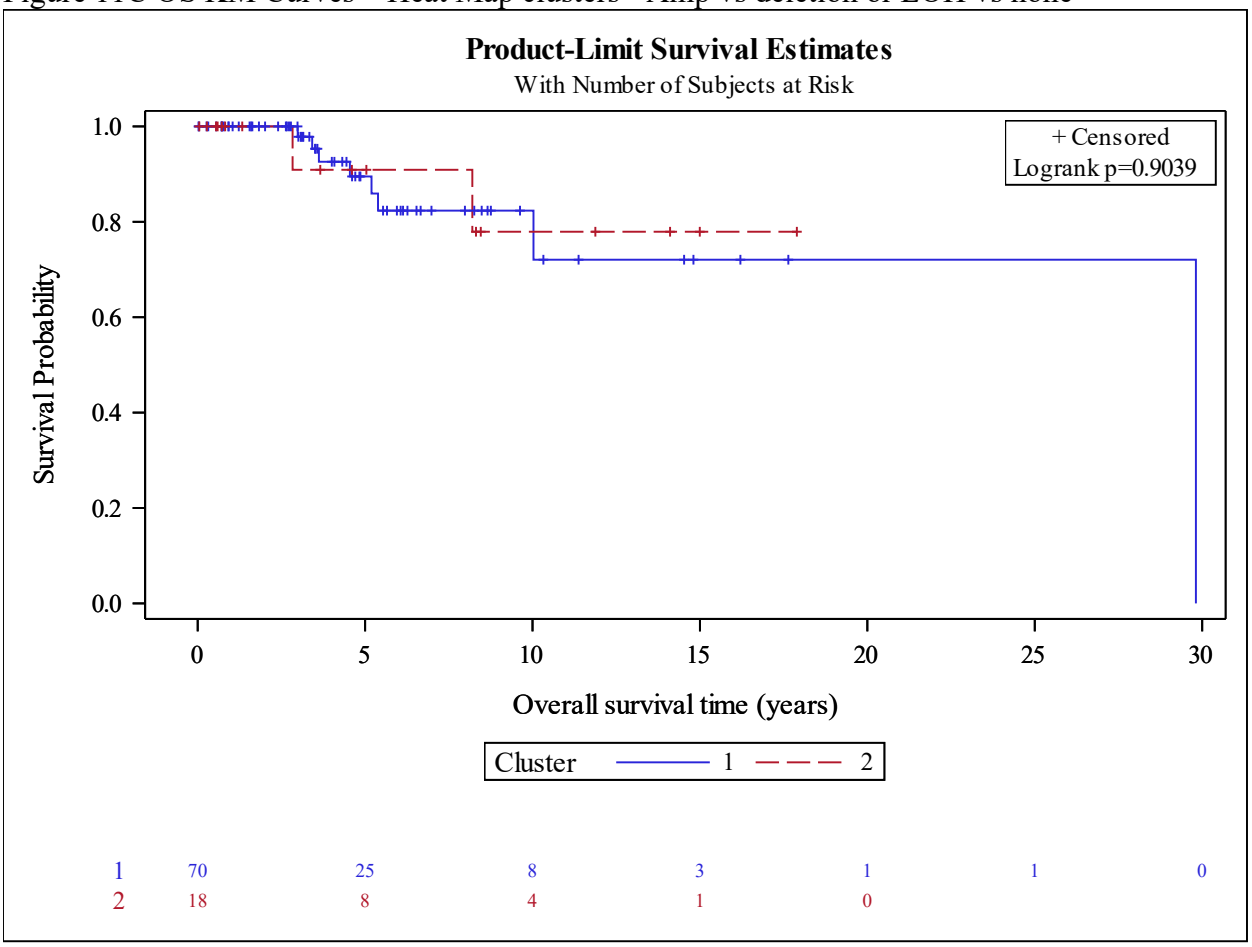

Cluster	No. of Subject	Event	Censored	Median Survival (95% CI)	1 Yr Survival	3 Yr Survival	5 Yr Survival	10 Yr Survival
1	70	8 (11%)	62 (89%)	29.8 (10, 29.8)	100.0% (NA, NA)	97.8% (85.6%, 99.7%)	89.5% (74.2%, 96.0%)	82.3% (64.3%, 91.8%)
2	18	2 (11%)	16 (89%)	NA (8.2, NA)	100.0% (NA, NA)	90.9% (50.8%, 98.7%)	90.9% (50.8%, 98.7%)	77.9% (35.4%, 94.2%)

Figure 12: Two example subjects demonstrating the results of preprocessing steps including denoising, biasfield correction, brain masking and intensity normalization.